REPORT DOCUMENTATION PAGE

Form Approved
OMB No. 0704-0188

1. REPORT DATE *(DD-MM-YYYY)*	2. REPORT TYPE	3. DATES COVERED *(From - To)*
18-11-2010		01 MAY 2009 - 28 FEB 2010

4. TITLE AND SUBTITLE

Non-Thermonic Cathode for High Power Long Pulse, Long Lifetime Magnetrons

5a. CONTRACT NUMBER
FA9550-09-C-0127

5b. GRANT NUMBER

5c. PROGRAM ELEMENT NUMBER

6. AUTHOR(S)

Dr. Miles Collins Clark

5d. PROJECT NUMBER

5e. TASK NUMBER

5f. WORK UNIT NUMBER

7. PERFORMING ORGANIZATION NAME(S) AND ADDRESS(ES)

Collins Clark TEchnologies Inc.
3738-C Hawkins St. N.E.
Albuquerque,
New Mexico 87109

8. PERFORMING ORGANIZATION REPORT NUMBER

9. SPONSORING / MONITORING AGENCY NAME(S) AND ADDRESS(ES)

AFOSR875 N RANDOLPH ST
SUITE 325
ARLINGTON, VA 22203

10. SPONSOR/MONITOR'S ACRONYM(S)

11. SPONSOR/MONITOR'S REPORT NUMBER(S)
AFRL-OSR-VA-TR-2012-0002

12. DISTRIBUTION / AVAILABILITY STATEMENT

Approved for public release; distribution is unlimited.

13. SUPPLEMENTARY NOTES

14. ABSTRACT

Report developed under STTR contract for topic AF08-BT14.
There is considerable interest in adapting the conventional Magnetron Oscillator tube for use in High Power Microwave applications. A major obstacle in this is that the conventional thermionic cathode doses not provide acceptable electron emission for operation in the HPM power levels (> 100Mw). In this work, we explore the potential for using arrays of sharpened microscopic carbon fibers to provide field emitted electrons at room temperature and without plasma generation. This study builds on previous work with single carbon fibers in which adequate cold emission was observed.
We describe experimental results in which ~ 1 cm2 arrays containing approximately 10,000 individual fibers were studied. Initial explosive emission (including plasma formation and diode shorting) was observed. Careful conditioning techniques were developed to suppress this process and to eventually produce very long pulse (~ seconds), uniform field emission. The effects of pulse rise time, diode vacuum, Cesium Iodide coating and emission field levels are discussed. Finally, the results of 3 dimensional particle-in-cell simulation of a Magnetron tube geometry are described.

15. SUBJECT TERMS

STTR REPORT

16. SECURITY CLASSIFICATION OF:			17. LIMITATION OF ABSTRACT	18. NUMBER OF PAGES	19a. NAME OF RESPONSIBLE PERSON
a. REPORT	b. ABSTRACT	c. THIS PAGE			Dr. Miles Collins Clark
					19b. TELEPHONE NUMBER *(include area code)* 505-263-7036

FINAL TECHNICAL REPORT
AFOSR CONTRACT: FA9550-09-C-0127

"Non-Thermionic Cathode for High Power Long Pulse, Long Lifetime Magnetrons"

Miles Collins Clark, Ph.D.

owner/president

Collins Clark Technologies Inc.

Albuquerque, New Mexico

Edl Schamiloglu, Ph.D.

Professor

University of New Mexico

Albuquerque, New Mexico

1.0- INTRODUCTION:

High power microwave tubes are an important technology for use in directed energy systems. In a conventional Magnetron tube (**figure 1**), electrons are supplied by tunneling from a heated, low work function cathode. With proper choice of material, temperature and geometry, emission current densities > 10 amps/cm^2 and total currents >100 amperes are possible.

Heating the cathode to these temperatures requires an external power supply which must be operated at the cathode potential (~10-50kV). Typically, this isolation is obtained via an isolation transformer, requiring an AC filament power supply. The added complexity of this circuitry along with the thermal management considerations increases system size and weight and limits lifetime. Scaling to higher current (and hence higher power) operation for possible military applications is

possible only by increasing the filament temperature. Advanced tube concepts such as multi beam or inverted designs are limited due to the difficulty of increasing emission area.

The goal of this STTR topic is to develop a cathode structure which operates at ambient temperature. A conceptual Magnetron employing an unheated cathode is shown in **figure-2**. Here, the electrons are produced by field emission from micro-fibers covering a cathode surface. The electron emission is controlled by a voltage between the cathode and a semi-transparent grid. Electrons attracted toward the grid are injected into the Magnetron interaction region. The power required to supply this extraction voltage is provided by picking off the high voltage supply rather than from an external circuit. Unlike the heated cathode, no power is required between pulses. This "cold" cathode will allow higher current operation, longer lifetime, reduced cooling power and greater simplicity by eliminating the heater and support circuitry. In addition, by controlling the emission (in this case through the use of an extraction grid) the tube can be turned on and off (gated) thus reducing or eliminating the need for external pulsed forming circuitry. In essence, the tube itself acts as the pulsed forming circuitry (a hard tube modulator). Finally, by eliminating the need to heat the electron source, it should be possible to produce very large emission structures of arbitrary geometry for use in high power and advanced tube concepts such as the inverted magnetron. This topic has a performance goal of 1-10amps/cm^2 for an emission area of 10-100 cm^2 and a phase-2 demonstration goal of 10 amperes in pulses of >=10ms. These goals are consistent with the parameters of the existing California Tubes Laboratory CTL-300 magnetron tube

The pulsed mode CTL 300L tube has the following parameter:

- ~20 amperes total current
- ~70 cm^2 emission area =>300ma/cm^2
- 50 ms pulse width

- 10 Hertz pulse repetition rate (50% duty cycle)
- 1000 hours lifetime.

2.0 OVERVIEW:

The critical issue in determining if long pulse, high current density electron emission can be achieved with cold emission sources is the elimination or reduction of plasma formation in the source material. Building on past work with single carbon fiber samples we need to demonstrate scaling of these single fiber results to large area emission. While the ultimate application is to the Magnetron tube, that geometry is sufficiently difficult to construct and diagnose that we have chosen to first explore electron emission in a planar, non magnetized geometry. This planar geometry makes it possible to analyze and test a variety of configurations within the scope and limits of this phase -1 effort.

In anticipation of ultimately moving to the actual magnetron geometry, a portion of work in this phase-1 effort was also dedicated to coaxial, magnetized extraction. Experimentally, the hardware was designed and constructed for coaxial magnetized extraction tests. In addition the simulation effort was completely dedicated to this geometry. It was anticipated that the planar geometry would answer experimentally the issues of plasma formation and area scaling and that the major effort would be later involved in the coaxial geometry. We couldn't afford to go immediately to the magnetron geometry and risk failing to achieve the basic understanding for feasibility. The entire effort could possibly be spent in hardware fabrication and testing without testing fiber emission scaling.

3.0 APPROACH:

The primary goal of this phase-1 effort was to determine feasibility of the final magnetron cold cathode. We decided that only the most critical issues would be studied in order of importance. Since plasma formation is at the basis of this concept, a primarily experimental effort was called for. Plasma formation has been the core physics of high power diodes and it is a complicated process. We felt that time spent on experiments, diagnostics, sample tests, etc was far more important at this initial phase than theoretical work. As a practical matter, we felt that it was important to attempt scaling of existing single fiber results up to practical sizes (~1 cm^2). On the other hand, we felt that some effort toward the final goal was required. This led to the project path outlined in **figure 3**. Here, we show the move from existing single fiber results to a carefully prepared array of fibers. This report is structured in the sequence of work performed. Although hardware was constructed for the coaxial, magnetized experiments, time and budget constraints limited the work to the planar geometry. The coaxial hardware: magnet system, vacuum insulator, cathode and grid holder etc. are available for future work.

4.0 OBJECTIVES:

5.0 WORK CARRIED OUT:

5.1 PULSED POWER SYSTEM:

The conventional, repetitive generator incorporates a PFN at high impedance or a liquid dielectric transmission line at low impedance to produce the desired waveform. These systems are inherently complex and bulky. Explosive pulsed power is low impedance, simple and compact but is limited to

specialized, single shot applications. In addition, a nonlinear element (typically a fuse) is required to condition the wave shape and transfer power to the load. These pulsed power systems typically drive charged particle beam diodes based on explosive emission which inherently present a time varying impedance due to plasma generated in the emission process. This collapsing impedance requires a trade off in generator design to maintain a reasonably constant voltage while matching power to the diode. The PFN internal impedance must be matched to that of the load to prevent reflection and perturbation of the waveshape. The typical solution to this problem is to design the PFN to have an internal impedance substantially lower than that of the diode and then to install a parallel resistance so that a reasonably match is presented to the generator.

Although surge arrestors have been used in the past to attempt pulse shaping[1] , we have found that by replacing this parallel resistance with a surge arrestor, not only is a constant impedance achieved but the need for the PFN itself is eliminated. While we are still in the initial process of understanding the advantages and limitations of this approach, we are routinely using it in ongoing diode research and are developing a line of commercial systems based on this concept.

5.1.1 CONCEPT

Although this technique is very simple in both concept and practice, it is non-intuitive (at least to the author) and requires some effort to understand. It was some time after thinking of the idea (preventing voltage surges in laptop computers and producing flat pulses for pulsed power applications are similar problems) that a design technique was developed. This paper is structured in roughly the sequence that was followed, from empirical simulation through development of a design criterion to full scale experiment.

Consider first the simple circuit shown in **figure 4**. This LRC circuit is the most basic pulsed power system. The capacitor (C) is typically a Marx Generator which delivers energy through the inductance (L) to the load resistance (R) when the switch is closed. This efficiently delivers energy to the load but with no waveshaping.

Now, consider the circuit shown in **figure 5**. Here an ideal Zener Diode replaces the load resistor. This ideal device is open circuit until its characteristic clamp voltage (V_{zener}) is reached. At this point its dynamic resistance becomes zero. In the simulation, if the initial charge voltage exceeds V_{zener}, then the circuit conducts current, the capacitor discharges and the diode voltage is clamped. The pulse width is determined primarily by the LC period and the ratio of charge voltage to V_{zener}. In fact, it is easy to demonstrate that by "tuning" the inductor value, it is possible to adjust the pulse width. Note also that in this idealized example, the dynamic impedance of the system is zero and it is extremely "stiff".

We now modify this still idealized circuit so that power can be delivered to a resistive load. We do this by inserting an output switch and a resistor as shown in **figure 6**.

As before, the main switch closes, driving current through the diode which clamps the voltage at V_{zener}. After a selected time delay during which the zener current continues to rise, the output switch is closed.

With the load resistor and diode now connected in parallel, a portion of the current is effectively transferred from the diode to the resistor. The diode continues to clamp the voltage so long as some current flows through it no matter how little. In fact, the load resistor can have any value above

$Z = \sqrt{\frac{L}{C}}$ (the Marx Generator internal impedance) without changing the voltage significantly. The proper time to close the output switch is after the current through the diode has reached or exceeded that expected in the load resistor when transfer occurs.

This circuit, while very simple none the less demonstrates characteristics of the actual pulsed power system described later.

5.1.2 THE PRACTICAL CIRCUIT

A. MOV surge arrestor

Although the circuit described above is instructive, the Zener diode power handling capability is far too low to be of practical interest in pulsed power applications.

The solution is to use commercial surge arrestors like those shown in **figure 7**.

The surge arrestor[2-4] (typically a Metal Oxide Varistor or MOV) was invented in the 1970's by General Electric Corporation and is today used whenever electronic devices must be protected against power line surges. Surge arrestors are found in applications ranging from the spike protectors in household power strips, to large arrays capable of protecting entire power plants during megavolt lightning strikes. Connected across a power line, the MOV (like the Zener diode) presents a very high impedance to the circuit until a specific threshold voltage is exceeded. At this point it rapidly begins conducting (<50 nanoseconds) with characteristics of a forward biased diode ($I \sim V^{25-50}$).

The characteristic clamp curves for several of these devices are shown in **figure 8**. These devices operate over a very large current range, but are far from zero dynamic impedance.

A 2:1 voltage variation is typical over the full operational current range. This voltage variation is the fundamental issue in commercial surge protection as well as in the present pulsed power application.

It should be noted that this application is considerably simpler than that of lightening strike protection. We know the characteristics of the Marx Generator precisely while a lightening strike is highly variable.

B. Circuit Simulation and Operating Point Calculation

The first attempt at simulation was to follow the empirical technique used earlier. The curves in figure 8 are digitized and then converted to ordered V,I pairs. To obtain other operating voltages, the single chip data are multiplied by the number of chips. These ordered pairs are then entered into the functional current source available in MICROCAP®, I=f(V). The circuit of **figure 9** is the

result. It was quickly discovered however that this empirical approach was no longer useful. A wide range of waveshapes (most of them unusable) would result from minor parameter changes. This is clearly due to the finite dynamic impedance of the MOV. Some method of obtaining the circuit operating point was required.

It was found that the simplest technique for obtaining the operating point was to solve for it graphically. As seen in **figure 10**, once the output switch if closed, the MOV and load resistor are in parallel. Prior to that, the MOV is the total Marx load.

This graphical solution was accomplished utilizing a commercial analysis and acquisition package (IGOR™ available from Wavemetrics® Corp). An example of the screen is shown in **figure 11.**

Here, along with the Marx Generator load line can be seen the load and MOV impedance curves. The parallel combination of load and MOV are then calculated and displayed. The operating points are where the various impedances intersect the load line.

In practice, all data is entered through a set of sliders and knobs in IGOR™ and the curves adjust to these changes in real time. In this way it is a simple to change MOV stack height, charge voltage, etc. and immediately observer the effect on the operating point. Note that in figure 11, the operating point prior to connecting the load is at a somewhat higher voltage than with the load connected. This is the result of the finite dynamic impedance of the MOV chips.

When a suitable operating point is established using this approach, the resulting MOV data are converted to (V,I) ordered pairs and transported into the MICROCAP® simulation.

Figure 12 shows the simulation results using this process along with data from **Table-1**.

This simulation was used to construct the demonstration pulser described below. The switch out time in the simulation was chosen to correspond to that of the self break switch in the experiment.

5.1.3 THE AFOSR PULSER:

In order to test the validity of this design process and to demonstrate the operation of this concept, a moderately low power pulser was constructed and is shown in **figure 13**. Pulser parameters are listed in table-1. This is a fully functional pulser and is currently being used in CCT studies of long pulse field emission cathodes.

It consists of several components developed by CCT. These include a solid state switch capable of 40 kilovolt, 500 ampere operation (model SSW-403) and a gas insulated field distortion switch capable of 200kilovolt, 50 kiloampere operation (Model GSW-204). The components are located in a 20 cm. diameter aluminum cylinder and are insulated with pressurized air.. The primary switch is optically triggered while the output switch is self break. The MOV stack is composed of a 10 element string of commercially available chips (Panasonic model ZNR10182). The voltage output is selected by connecting the output line to the proper number of chips (5 for these tests).

The capacitor is a Cerrento model 12312 40nF/100kV. The inductor is made from a spool of high voltage wire (Belden 88690101). The load is a 500 Ohm high voltage resistor. The circuit is wired together with standard automotive non-resistive spark plug cables. Load voltage is measured using a Northstar® model PVM-12 high voltage probe and the MOV current is measured with a current viewing resistor. The system is located in a Lingren shield room and data acquisition is with a Tektronix 2024 digitizer. Operating parameters for these tests are shown in table 1.

Test data are shown in **figure 14**. Since the output switch was self-break for these tests, there was considerable jitter in the timing and this particular data set was selected for its optimal waveshape.

The risetime and voltage flattop are strongly dependent on this timing and we have subsequently installed a triggered output switch to stabilize this effect. Likewise, the switch-out time for the simulation was chosen to match the experiment. Note the close agreement between experiment and simulation. This validates the design process used.

A feature seen both in simulation and experiment is the slow trail off of the voltage after the MOVs stop conducting. This is a characteristic of the concept and can potentially cause problems in some applications. In this case, a crowbar switch is required.

An expanded view of the load voltage is seen in **figure 15**. The characteristic rapid transfer time from the MOV to the load results in a fast voltage rise time followed by the very flat waveform.

5.2 COAXIAL MAGNETIZED HARDWARE:

The coaxial, magnetized extraction assembly is shown in **figure 16**. On the left of the figure is a cutaway view of the SolidWorks© assembly showing the various components. The apparatus is constructed in standard NW-50 (2”) vacuum hardware which then adapts to the vacuum system. This will allow us to swap between the two configurations with minimal downtime. The fiber sample will form a strip in the coaxial cathode holder so that only a strip of beam will be extracted. This technique should limit the total amount of current extracted and allow better diagnostic and modeling capability.

5.2.1: Magnetic Field Coil:

The solenoid system has been constructed and is shown in **figure 17**. The coil itself consists of 500ft of #14 electrical wire with a 6 inch diameter bore. It is powered by an electrolytic capacitor bank (0.124 Farad, 300 volt) which is charged with a CCT fabricated power supply and switched with an SCR. The coil produces a 3 kG magnetic field with a 20mS critically damped waveform. This is sufficient to allow flux penetration into the stainless coaxial hardware.

5.3 Planar non-magnetized hardware:

We will begin the experiment with the hardware shown in **figure 18**. it is constructed of aluminum and uses Plexiglas cylinders for insulation and vacuum seal. A 1 cm. diameter fiber disk is mounted at the center of a 3" support plate. The grid is 90 % transparent stainless steel mesh mounted in a drumhead type stretcher ring. The anode is at ground potential and contains a graphite plate (not shown) which acts as both a beam dump and Faraday cup. The package mounts to standard NW-100 vacuum hardware as shown.

5.4 Laser triggering:

One of the effects that we want to explore is the importance of voltage rise time on emission from the fiber bundle. In the conventional explosive emission process, the fast rising voltage pulse produces a displacement current which charges the inherent stray capacitance associated with the fiber geometry. The resulting discharge of this stored energy causes plasma formation and electron emission. While providing a zero potential sea of electrons, the resulting plasma expansion (1-10

cm/μs) limits usable pulse lengths to a few microseconds at most and is not suitable to this application.

In order to study this effect, it is necessary to provide a precisely controlled voltage pulse rise time. The inherent rise time of the pulser is determined by the characteristics of the solid state switch used and is approximately 600 nanoseconds as shown in **figure 19**.

The pulse rise time is adjusted by modifying the basic pulser circuit to include a resistor-capacitor load and an output switch as shown in **figure 20.**

By inserting the R-C components, the pulser output in integrated and the rise time is controlled over a large range up to ~ 60 μS. In practice, the capacitor is composed of a set of 10 solidstate "doorknob" 2 nanofarad capacitors arranged in parallel as seen in **figure 21**. For slow rise time tests, the output switch is shorted out so that the load is directly connected to the RC package. Adding or removing capacitors with a fixed resistance of 3000 Ohms provides rise time steps from 6-600μS. A typical slow rise time (40μS) is shown in **figure 22**.

To achieve a very fast rise time, an output switch is inserted as shown in **figure 23**. It consists of two hemispherical stainless steel electrodes threaded on 1/4-20 screws for gap adjustment. Because we are operating at low voltage, there is no need for a pressurized housing and the switch is operated at ambient air pressure.

The switch must be triggered at a precise time in order to achieve a reproducible voltage level. This triggering is accomplished by illuminating the switch gap with ultraviolet light from a commercial

Nitrogen lase (Spectra-Physics© model 337-SI, 337.1nm, 75kW). This laser produces a 4 nanosecond light pulse with a total jitter from trigger to output of less than 30 nanoseconds. It is triggered from an external 5 volt logic pulse. The configuration is shown in **figures 24-25**,

The great advantage of using an ultraviolet laser pulse is it simplicity. Unlike optical laser triggering, there is no need to focus the beam to achieve adequate intensity. Rather, the unfocused beam (~0.4 cm^2) is directed between the electrodes as shown. This eliminates the need for complicated optics and greatly relaxes the alignment and positioning requirement. Using this technique, 15 nanosecond rise time pulses are achieved as shown in **figure 26**.

Here the RC charge voltage is shown along with the cathode voltage. These two techniques allow us to study the effects of voltage rise time from 15 nanoseconds to greater than 500 microseconds in a controlled and reproducible fashion.

6.0 RESULTS OBTAINED:

We have completed the research phase of this contract. Using a 1 cm^2 emitter we have demonstrated a >1μS, >10 amp beam with a plasma based emitter and 100 μS, ~1 ma emission without plasma. These results suggest that a long pulse, high power, cold cathode Magnetron is possible. Due to page limits, we will describe only those results most critical to evaluation of our progress toward this goal.

The purpose of this effort is to demonstrate a long pulsed, HPM Magnetron tube by developing an electron source with both high current capability and little or no plasma closure. The phase-1 work involves a small (<=1cm^2) disk of carbon fiber emitter situated in a planar, non-magnetized

configuration shown schematically in **figure 27**. This geometry is easy to fabricate, maintain and diagnose while permitting sufficient area and current for realistic scaling studies. The experimental setup (**figure 28**), is located in 10'x8' lab which is separated from the control and data acquisition area by a 12' distance. Addition of a telescope-CCD camera to view the emitter end-on proved extremely useful in diagnosing the non-plasma emission process.

The following discussion of experimental results will be organized in the rough order performed.. For all results presented here, significant conditioning was required to achieve stable behavior.

6.1 PLASMA BASED EMISSION/ PULSED CONDITIONING:

The first studies centered on the basic behavior of the carbon fiber disk under pulsed conditions. Since we are working with an extremely small extraction gap (3mm), the control of plasma expansion is critical to long pulse operation.

For this work the triode is operated in grounded grid mode (**figure 29**) and the total anode beam current is measured with a current viewing resistor. The voltage rise time is controlled by inserting a switch and capacitor as shown.

Typical behavior of a bare (not coated with Cesium Iodide) emitter is seen in **figure 30** where a 5kv/4amp beam is produced after breakdown at ~40kv/cm. with a plasma closure velocity of ~6mm/μS The oscillations in the voltage and beam current are due to transmission lines between pulser and experiment. Conditioning was accomplished by firing the pulser at 0.5 Hz. at a voltage set to produce diode arcing. The voltage was gradually increased until arcing ceased and uniform plasma formation was achieved (1000-5000 pulses).

The dependence on pulse rise time is shown in **figure 31** where it is varied from 15nS to greater than 3μS. It shows a small but definite **decrease** in threshold voltage as the voltage rise time is **increased**. This argues against capacitive breakdown effects and needs further study.

6.2 CESIUM IODIDE COATING:

The plasma emission studies were repeated after coating a new fiber sample with Cesium Iodide. The coating was applied in the standard, evaporative fashion. The emitter consists of bi-modal fibers, 90% are ~ 1mm high while the others are ~2mm high. **Figure 32** shows a micrograph of the freshly coated emitter with the spheres of CSI deposited on the fiber tips. The tall fibers (~20-50/mm^2) presumably account for the majority of emission.

As seen in **figure 33**, there is a significant decrease in plasma closure velocity and a corresponding increase in pulse width to >1μS. Note that the current follows the voltage for the pulse duration without any indication of gradual plasma closure. This suggests that the closure may come from localized edge effects rather than general plasma motion. If this can be demonstrated (with larger samples) then elimination of these edge effects may lead to a very significant pulse width increase.

6.3 NON-PLASMA EMISSION/DC CONDITIONING

These final experimental results are the most significant for achieving millisecond duration pulses. That is the complete elimination of plasma closure while maintaining uniform emission. For this, we employed a D.C. conditioning technique in which the cathode is grounded and a positive bias is applied to the grid with a +10kv/6mA power supply. The emitter is imaged end-on through the anode tube yielding the view seen in **figure 34**.

The D.C. conditioning process involved slowly increasing the voltage until arcing is observed. The switching power supply temporarily shuts down on each arc and automatically recovers in ~ 2 seconds. In this way, arcs are gradually eliminated (probably due to burn off of protruding fibers) and a steady emission current in achieved. The voltage is increased until arcs reappear and the

process is repeated until a maximum of +10kV is achieved. This total process generally takes 1-4 hours for each sample. **Figures 35-36** show frames taken from the digital video of this process. Figure 32 shows typical arcing during conditioning. Early in the process (1-2 hours) the arcs occur mainly at the "triple point" where the fiber and holder meet. Later (2-4hours) the arcs are distributed across the face of the emitter as well as at the edge. In addition, in this phase the arc frequency begins to significantly decrease from several per second to one or two per minute.

In between arcs, the fibers begin emitting a steady electron beam as measured by the current monitor in the power supply. At this time, the grid begins glowing due to beam heating. The IR sensitive CCD camera makes possible the images seen in figure 33. The grid heating provides a measure of the beam profile that was not possible with any other technique tried during phase-1. The left image shows emission from a small section of the disk (possibly only a single fiber) early in the conditioning process. At the end of the conditioning process, emission is seen over the full area of the disk and at substantially increased total current. The continued non uniformity suggests that emission is still coming from a small number of fibers distributed across the face but non-the-less clearly demonstrates area scaling. A demonstration that these D.C. results hold for pulsed operation can be seen in **figure 37**. While it is difficult to make current measurements at this level in a pulsed environment, one can clearly see beam current lasting for the >100μS pulse duration with no indication of plasma formation.

6.4 UNM 3-D PIC SIMULATIONS

Finally, the simulation effort at University of New Mexico is concentrating on the actual Magnetron geometry for the proposed phase-2 tube. **Figure 38** shows two runs at different magnetic fields for an extracted beam from a single emitter strip in the "A6" Magnetron geometry. In practice, there would be 6 strips arranged on a transparent type emitter. As can be seen in this

figure, the injected electron beam tends to re-enter the grid region in the absence of r.f. spoke formation. This effect is probably due to the fact that the electrons enter the Magnetron gap with non-zero energy (due to the extraction bias voltage) and thus have sufficient energy to make it back to the cathode. This effect will need to be studied in greater detail in a future effort.

7.0 TECHNICAL FEASIBILITY:

The experiments and numerical simulation accomplished in this phase-1 effort indicate that very long pulse, cold cathode emission is possible. Although this effort was necessarily limited in scope, the critical experiments demonstrated that plasma emission can be eliminated or greatly reduced by careful attention to field shaping geometry and proper conditioning techniques.

This latter point cannot be over emphasized. Only the simplest of conditioning techniques were possible in this effort but never the less "prepared" the emitter samples for uniform, non-plasma emission. Future work should include extensive investigation of the conditioning mechanism leading to the optimum conditioning procedure. This eventual conditioning procedure should be as automated as possible so that large area cathodes can be prepared.

8.0 SUMMARY:

The phase-1 scaled experiments suggest that a long pulse, cold cathode Magnetron is feasible. Conditioning techniques and procedures have been developed which permit cathode operation in both plasma generation mode and field emission mode.

In the plasma mode, > 10 amps/cm^2 at closure velocities < 2mm/μS were achieved using Cesium Iodide coated fibers, indicating that >1 μS HPM Magnetrons could be possible.

In the field emission mode, complete elimination of the plasma resulted in stead state emission at the milliampere level with the demonstration of area scaling. Additional work on both fiber design and conditioning techniques promise to increase area emission to ~ 1-10 amps/cm^2 for millisecond pulse operation.

REFERENCES:

[1] M. Giesselmann, T. Heeren, E. Kristiansen, J. Dickens, D. Castro, D. Garcia, M. Kristiansen, "Simulation, Design and Test of a MOV Pulse Shaping Device for High Power Microwave Generators" 1999 IEEE Pulsed Power Conference

[2] David B. Miller, Hong Bo Fan, Paul R. Barnes, "The Response of MOV and SiC Arresters to Steep-Front Longer Duration Current Pulses" 1990 IEEE Power Engineering Society Summer Meeting, Minneapolis, Minnesota, July 15-19, 1990

[3] Panasonic data sheet "ZNR®" Transient/Surge Absorbers (Type-D)

[4]General Electric "TRANQUELL™ Surge Arrestors Technical Data D61HFM 07/10/97

APPENDIX:

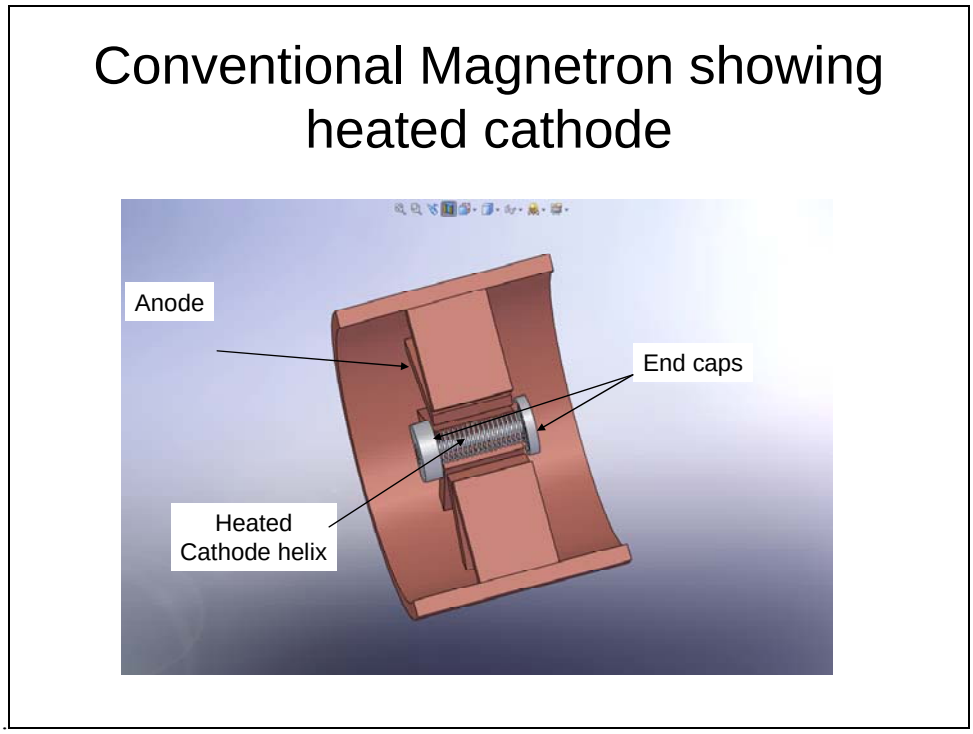

Figure 1 SECTION VIEW OF A CONVENTIONAL MAGNETRON

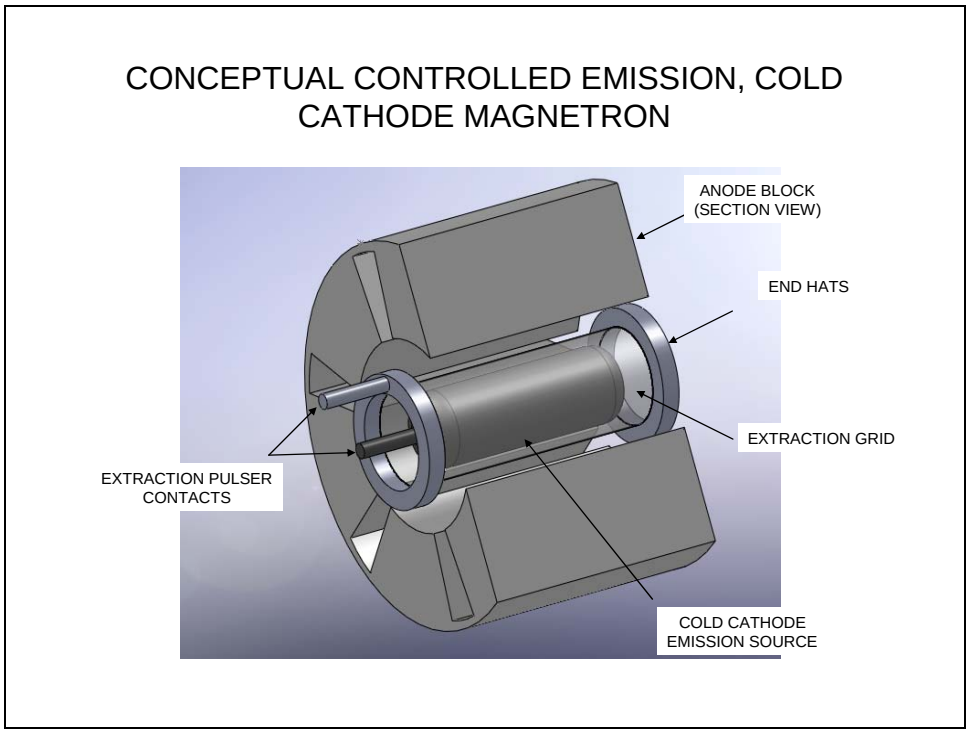

Figure 2 CONCEPTUAL COLD CATHODE MAGNETRON WITH GATED ELECTRON SOURCE

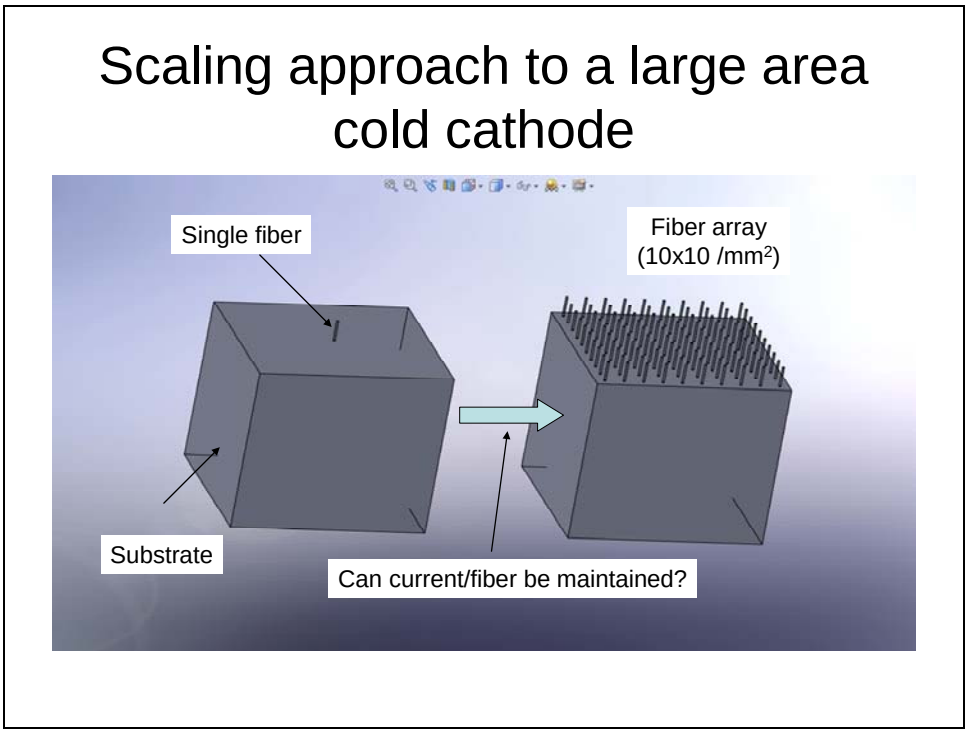

Figure 3 conceptual approach is to demonstrate fiber array emission

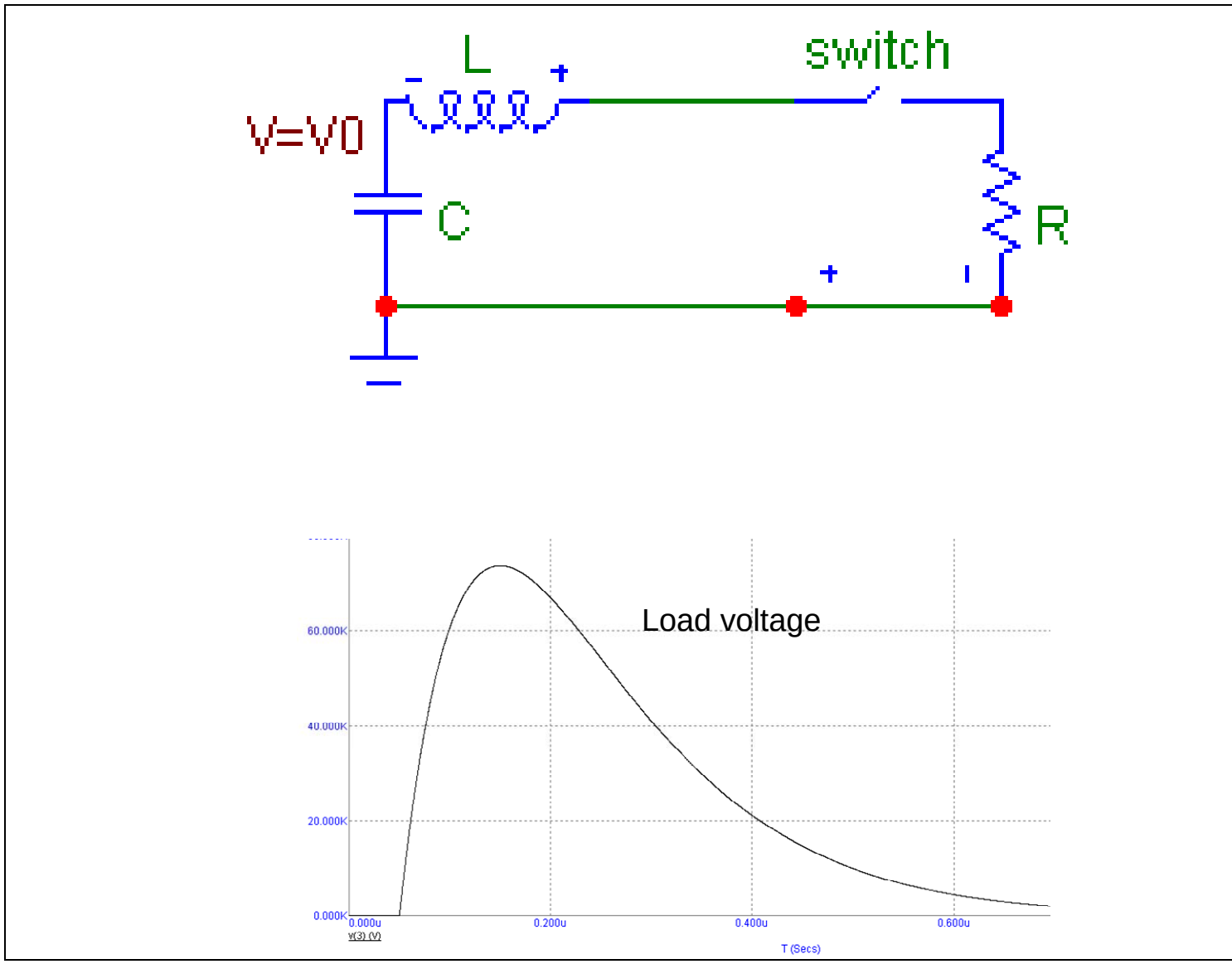

Figure 4. MICROCAP® simulation. LRC circuit (top). Load voltage waveform (bottom)

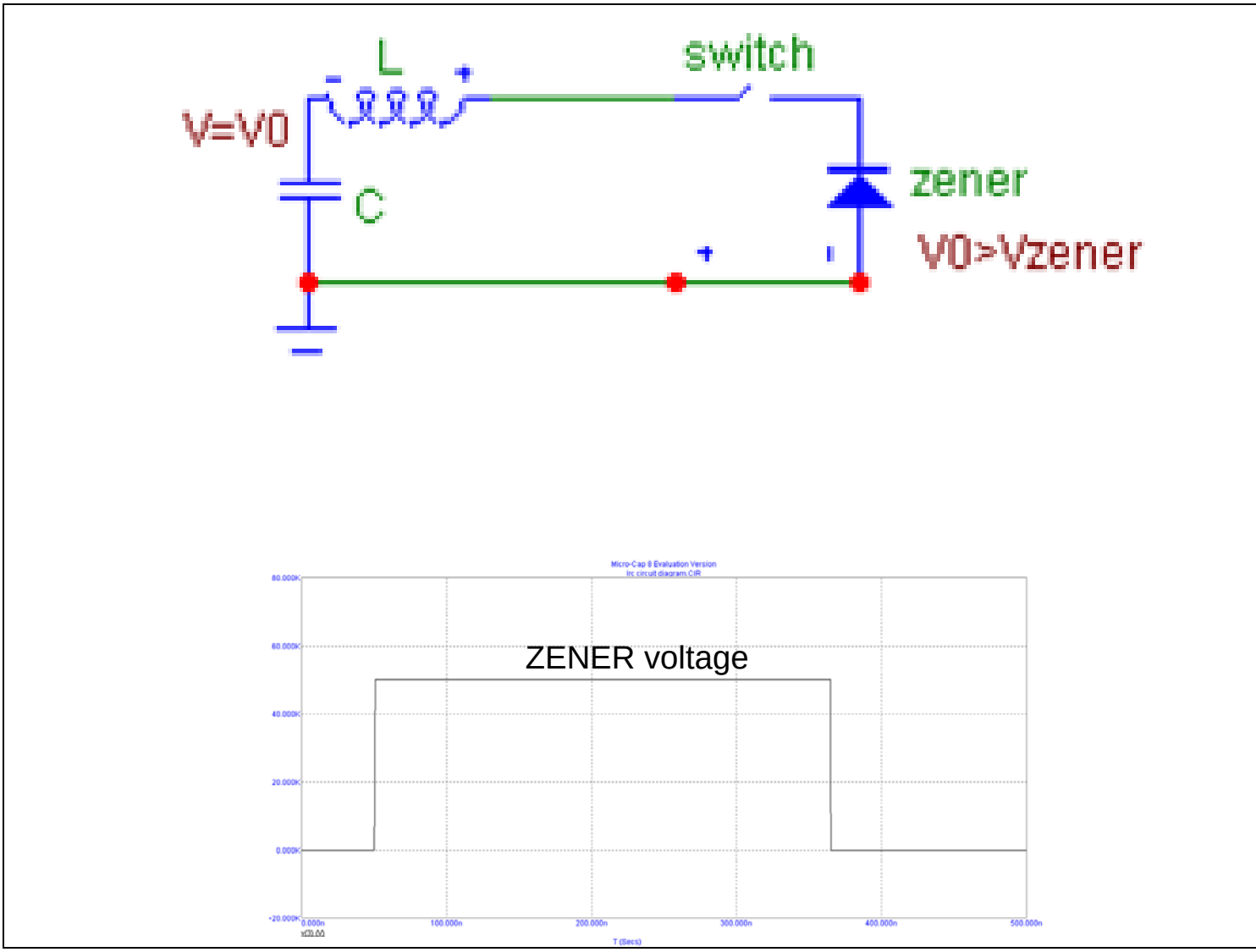

Figure 5 MICROCAP® simulation with a Zener diode replacing the load resistor

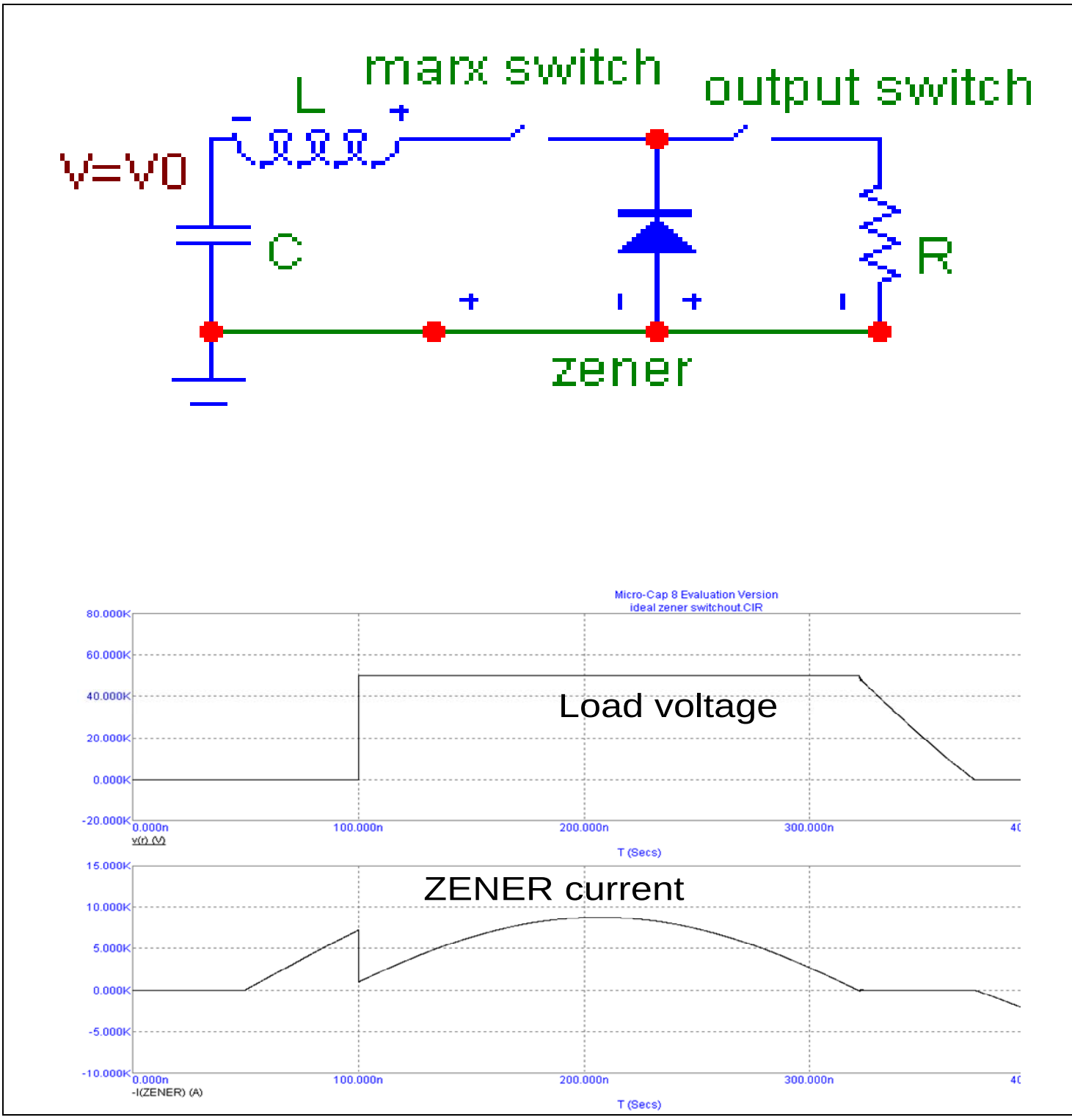

Figure 6 MICROCAP® simulation with a switch and resistor inserted

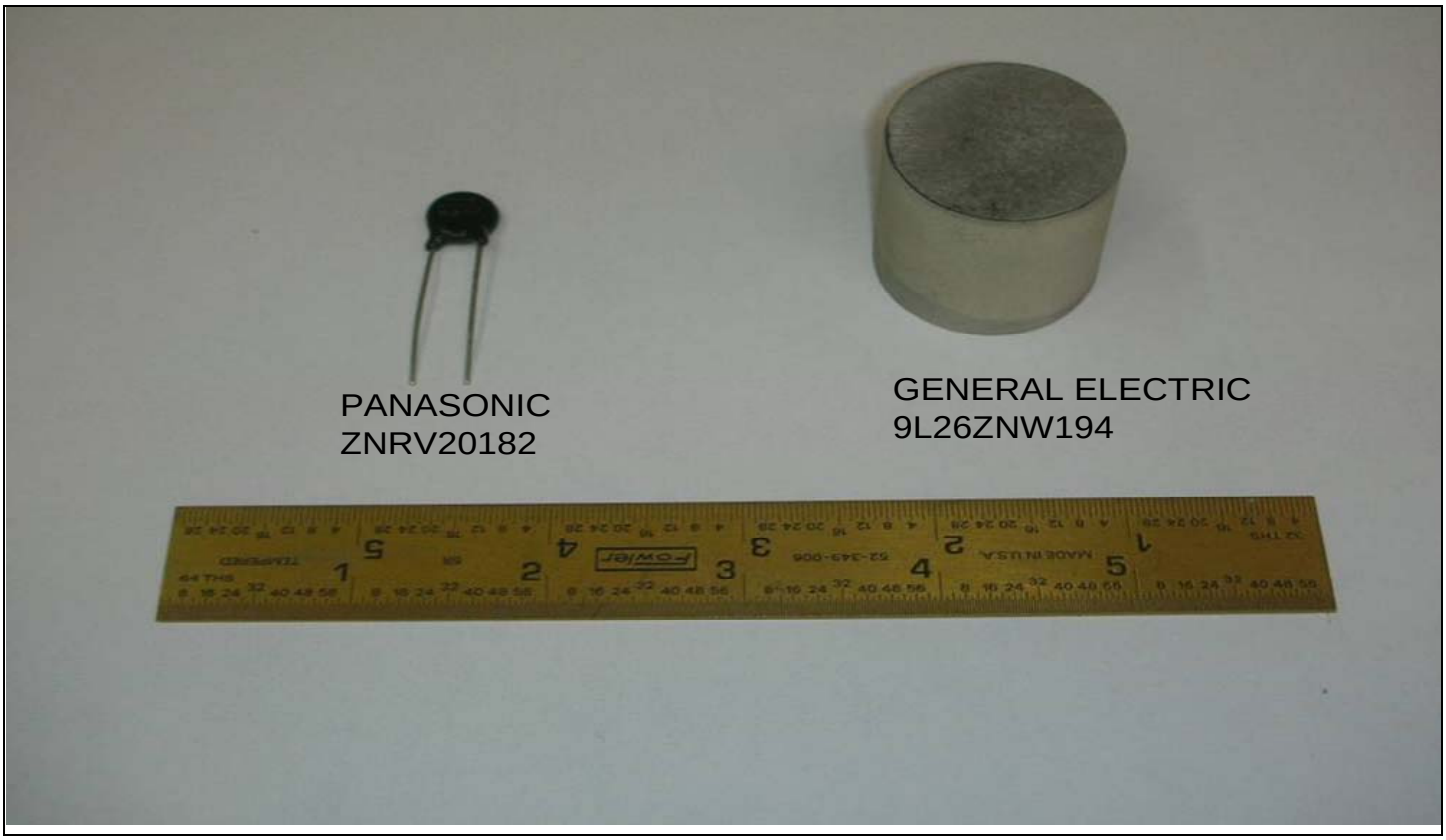

Figure 7 Commercial Surge Arrestor chips. Left: 2.5kV,1kA,1kJ. Right: 10kV,10kA,65kJ

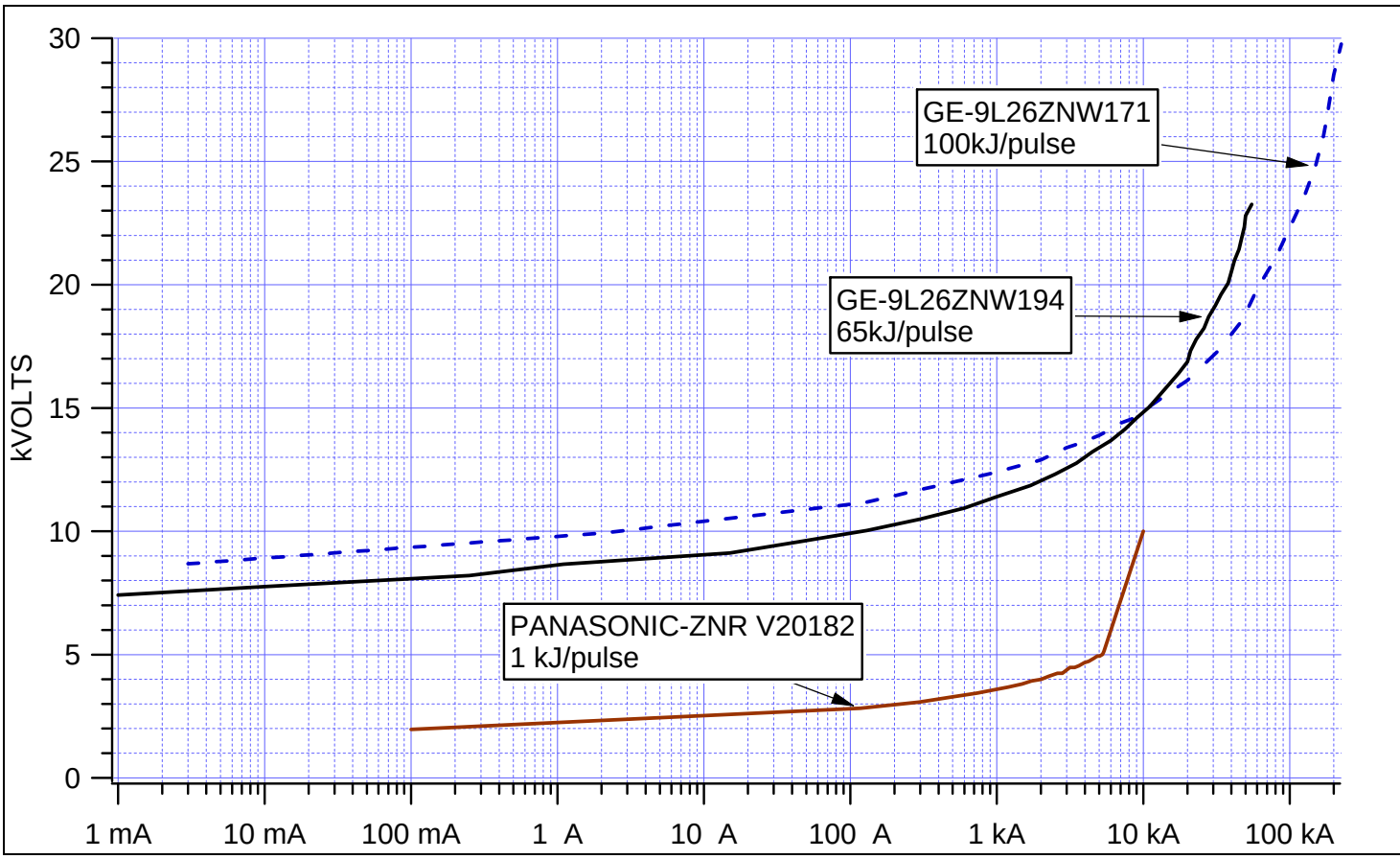

Figure 8 Curves for selected MOV arrestors

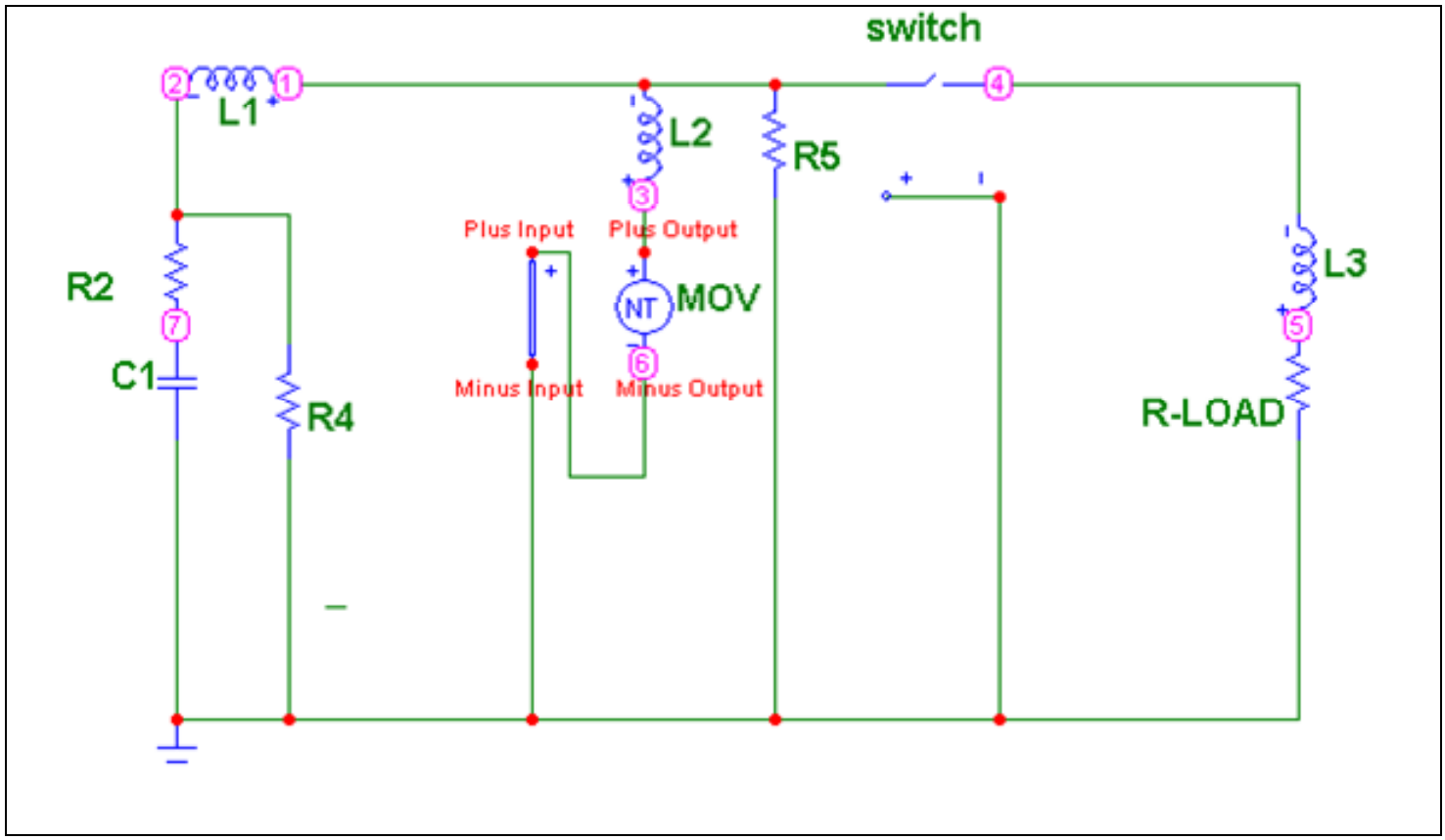

Figure 9 MICROCAP® simulation geometry using a functional representation for the MOV elements

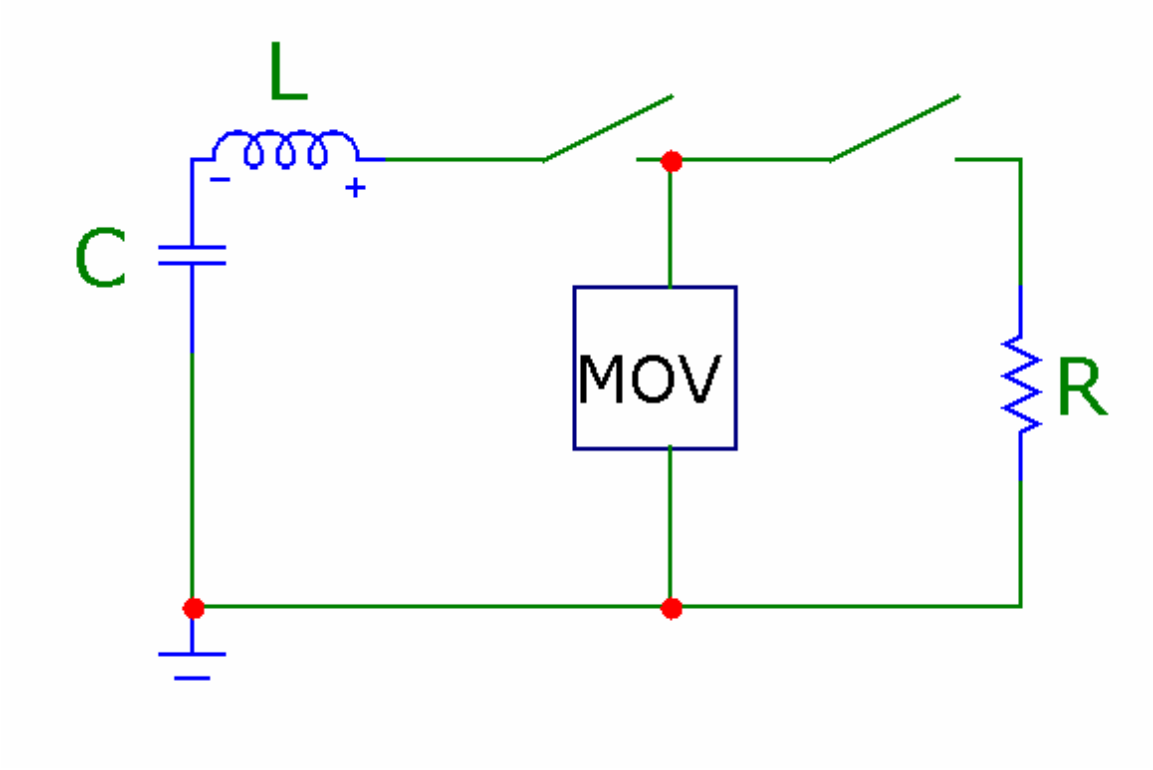

Figure 10 circuit model used to obtain operating point

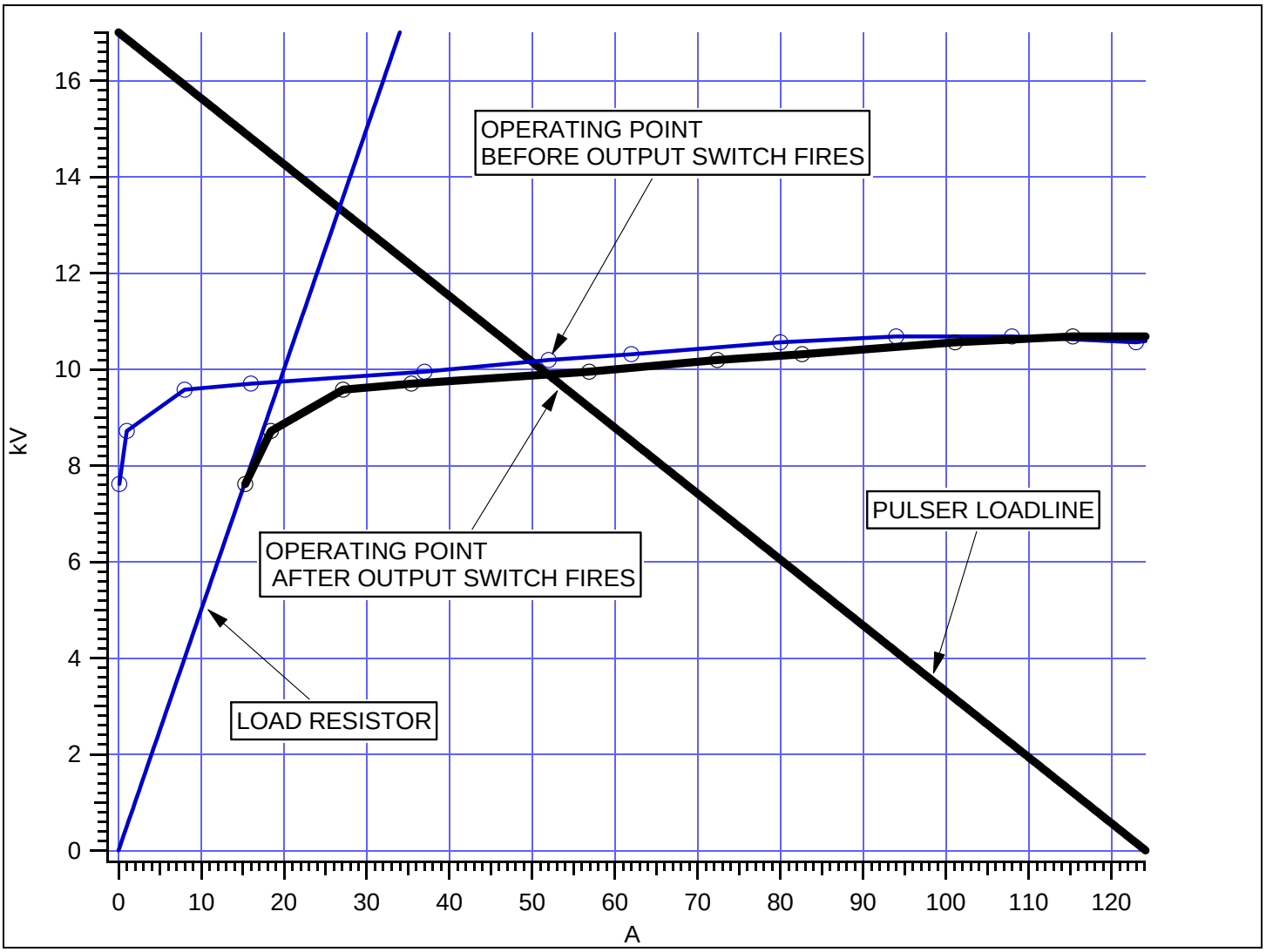

Figure 11. Graphical solution for the circuit operating point before and after connecting the load resistor.

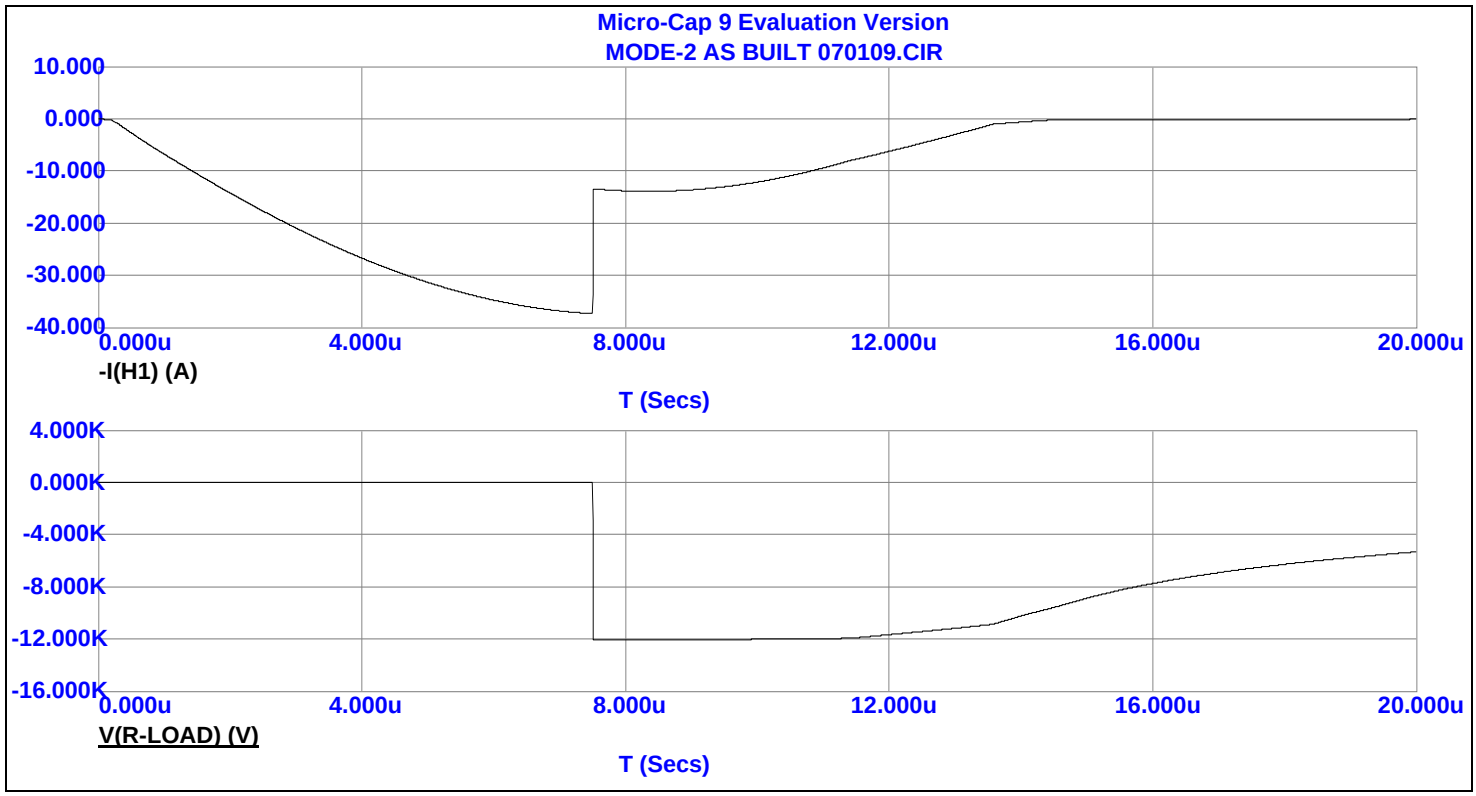

Figure 12 MICROCAP® simulation results. MOV current (upper), Load voltage(lower)

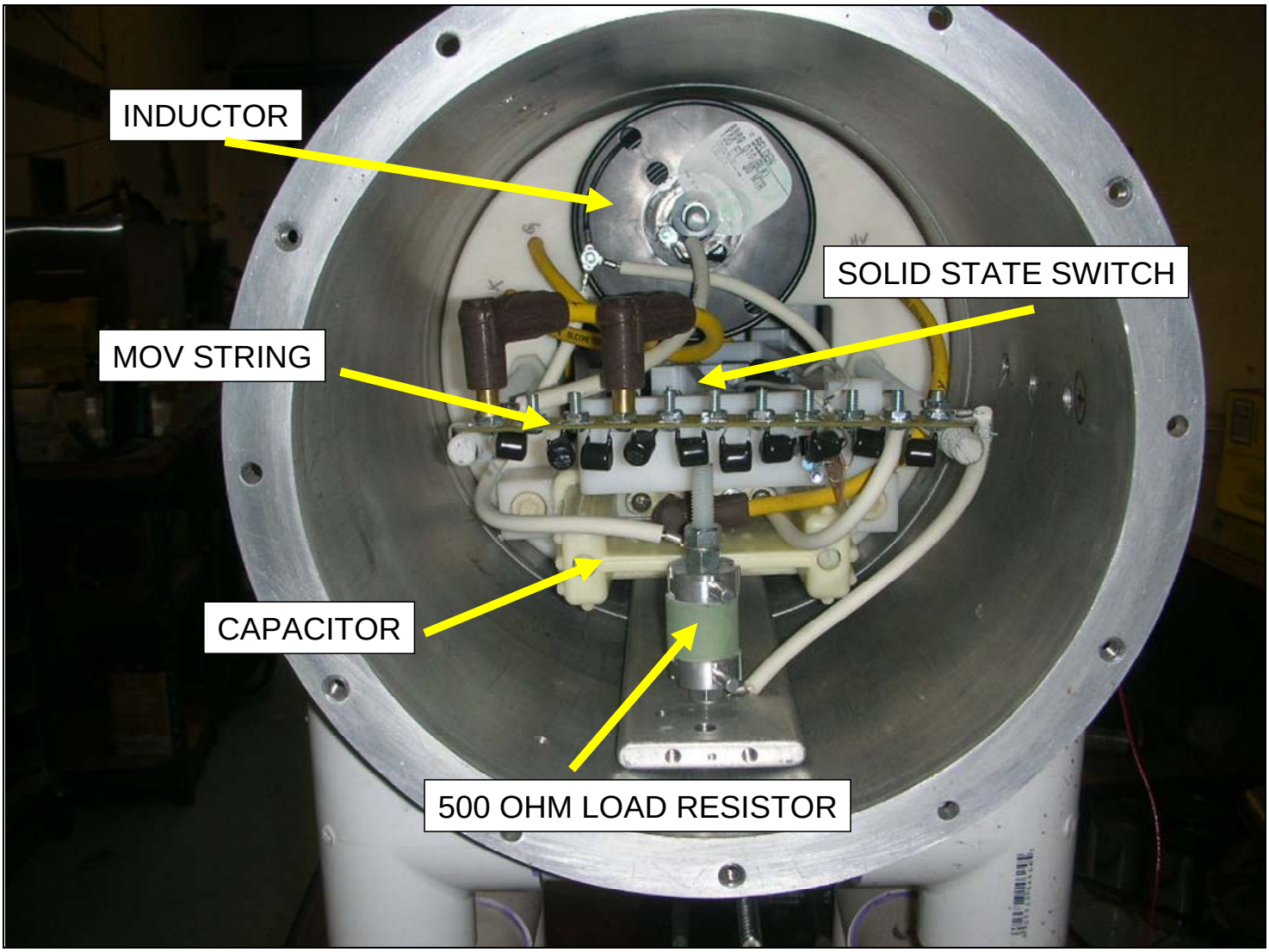

Figure 13 The Demonstration Pulser housed showing key components. The output switch is not shown in this view

Table 1. Demonstration Pulser Parameters

CHARGE VOLTAGE	18 KV (40kV max)
CAPACITANCE	40nF
INDUCTANCE	720uH
LOAD RESISTANCE	500 OHMS
MOV TYPE	ZNR10182
NUMBER OF MOVs	5 (10 max)
MARX SWITCH	SOLID STATE
OUTPUT SWITCH	GAS- SELFBREAK

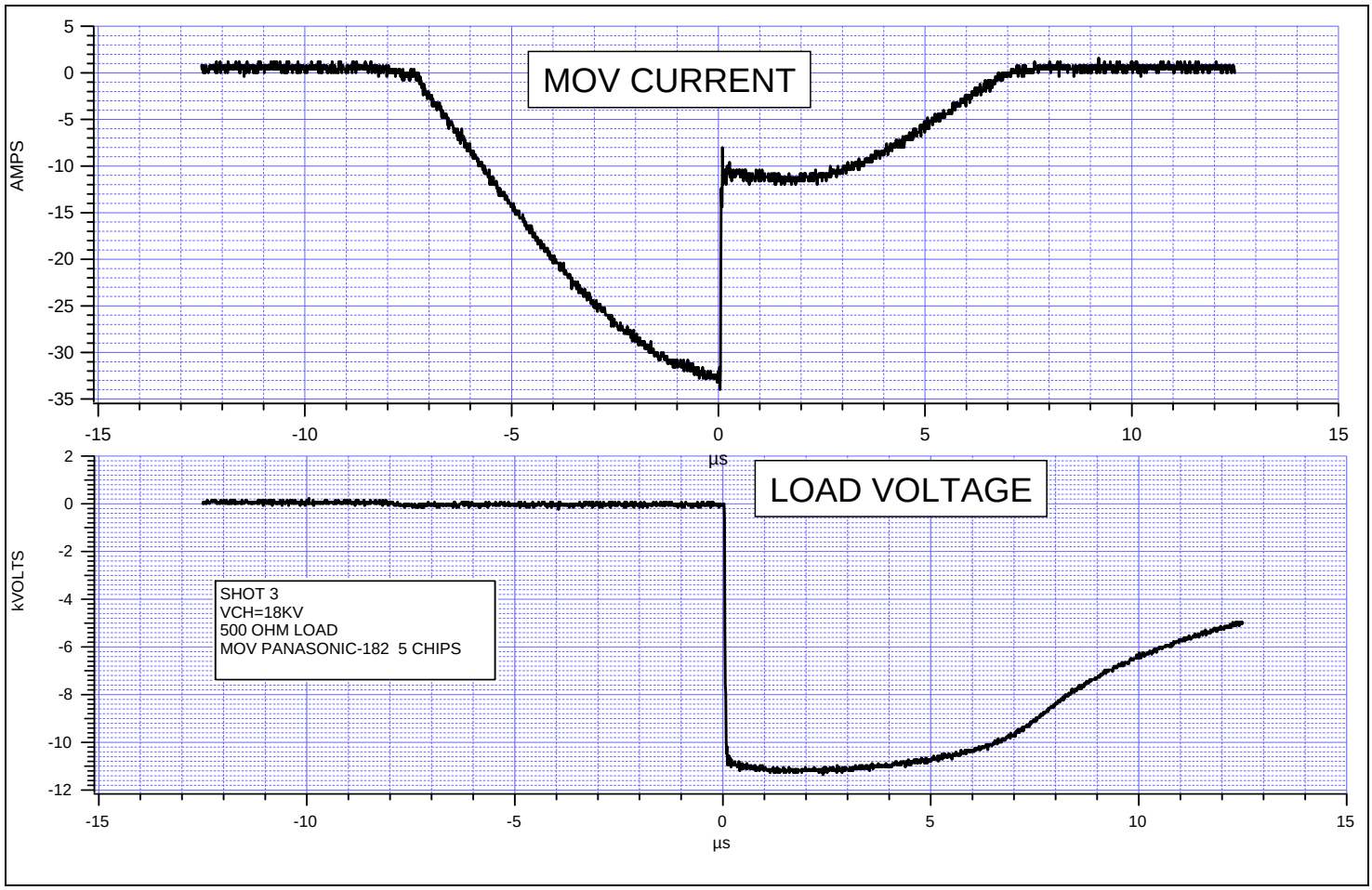

Figure 14. Demonstration Pulser data. MOV current (upper). Load voltage (lower)

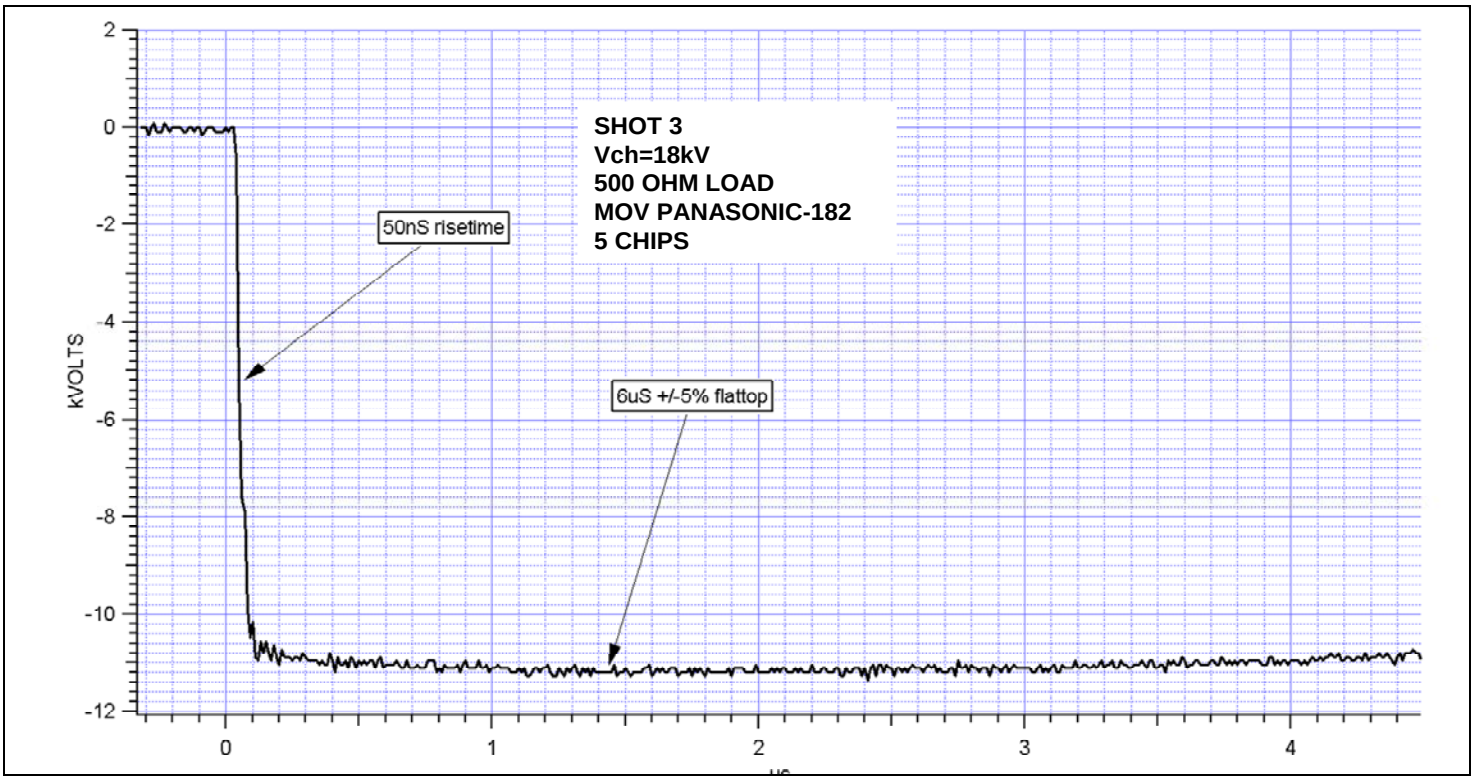

Figure 15. Load voltage showing fast rise and flat top

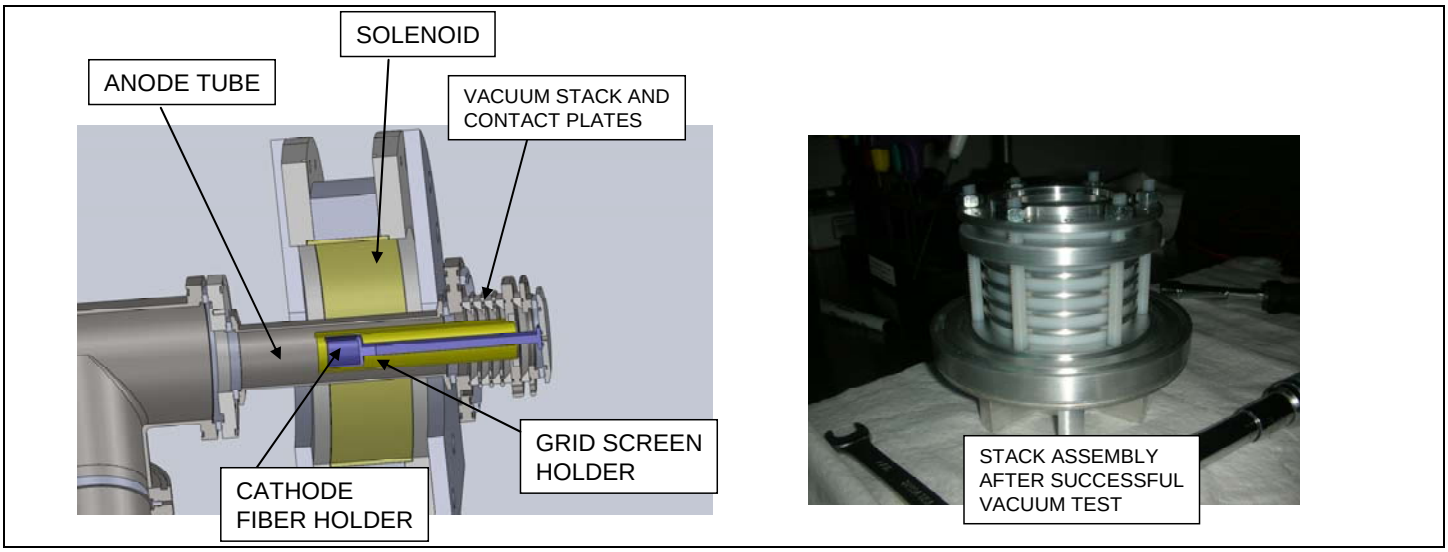

Figure 16. Magnetized coaxial assembly(l) and ring stack (r)

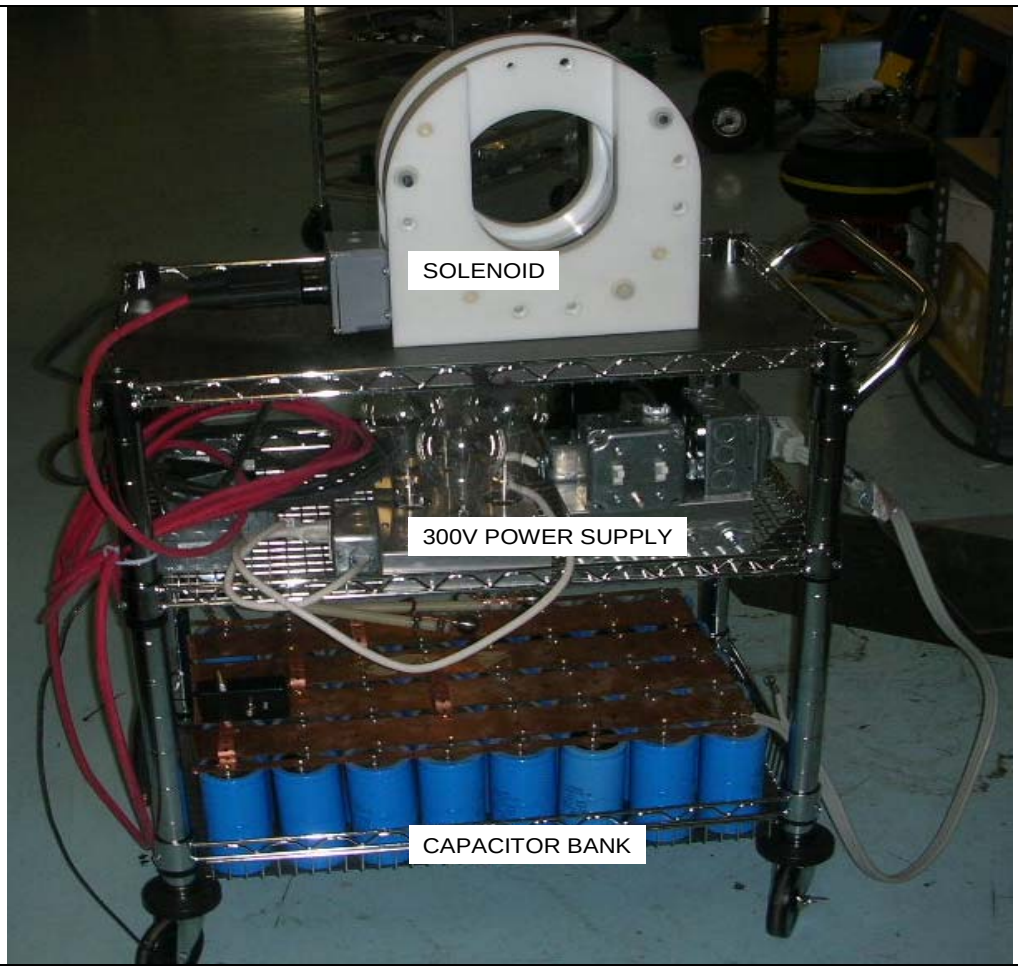

Figure 17. 3kG Magnetic Field System

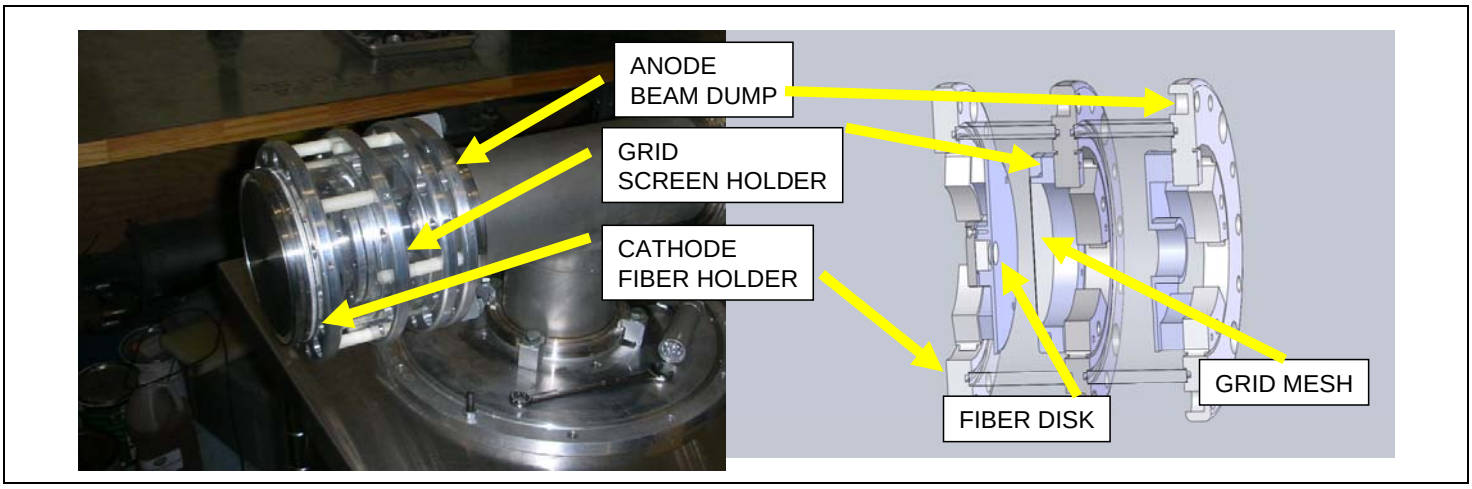

Figure 18. Planar Extraction assembly

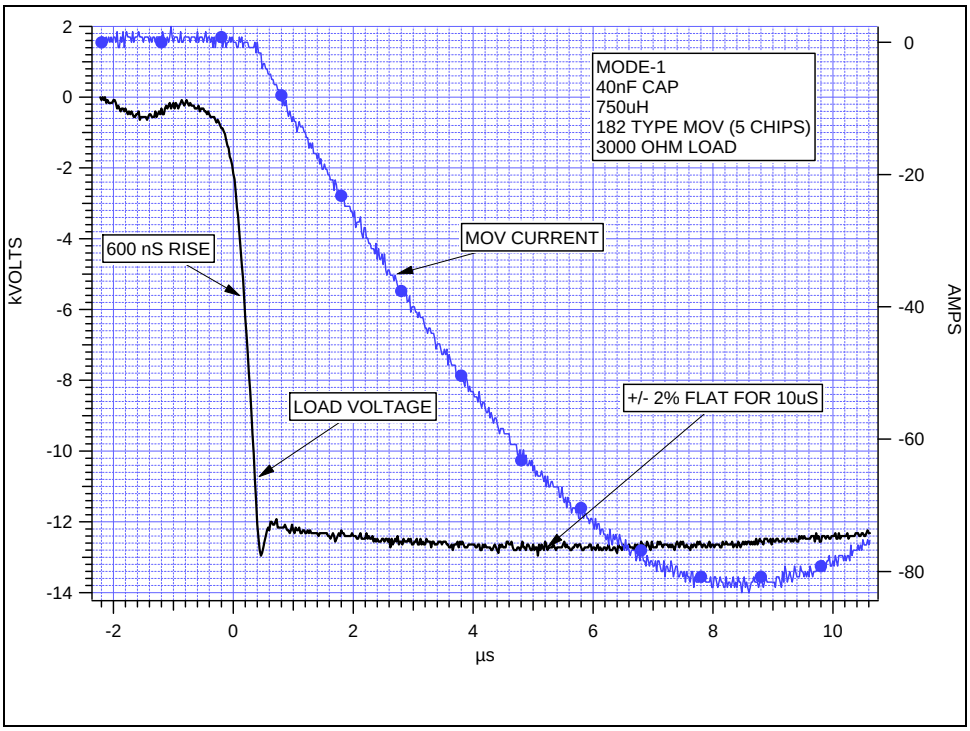

Figure 49 Inherent pulser rise time is ~ 600nS

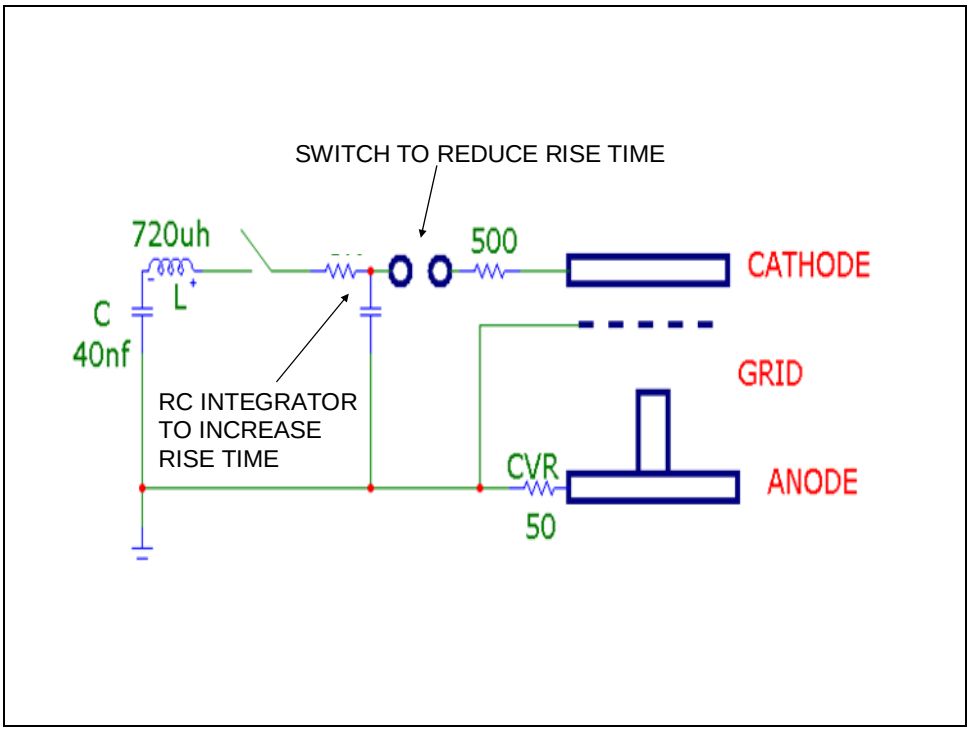

Figure 50 Modified circuit for variable rise time voltage pulse

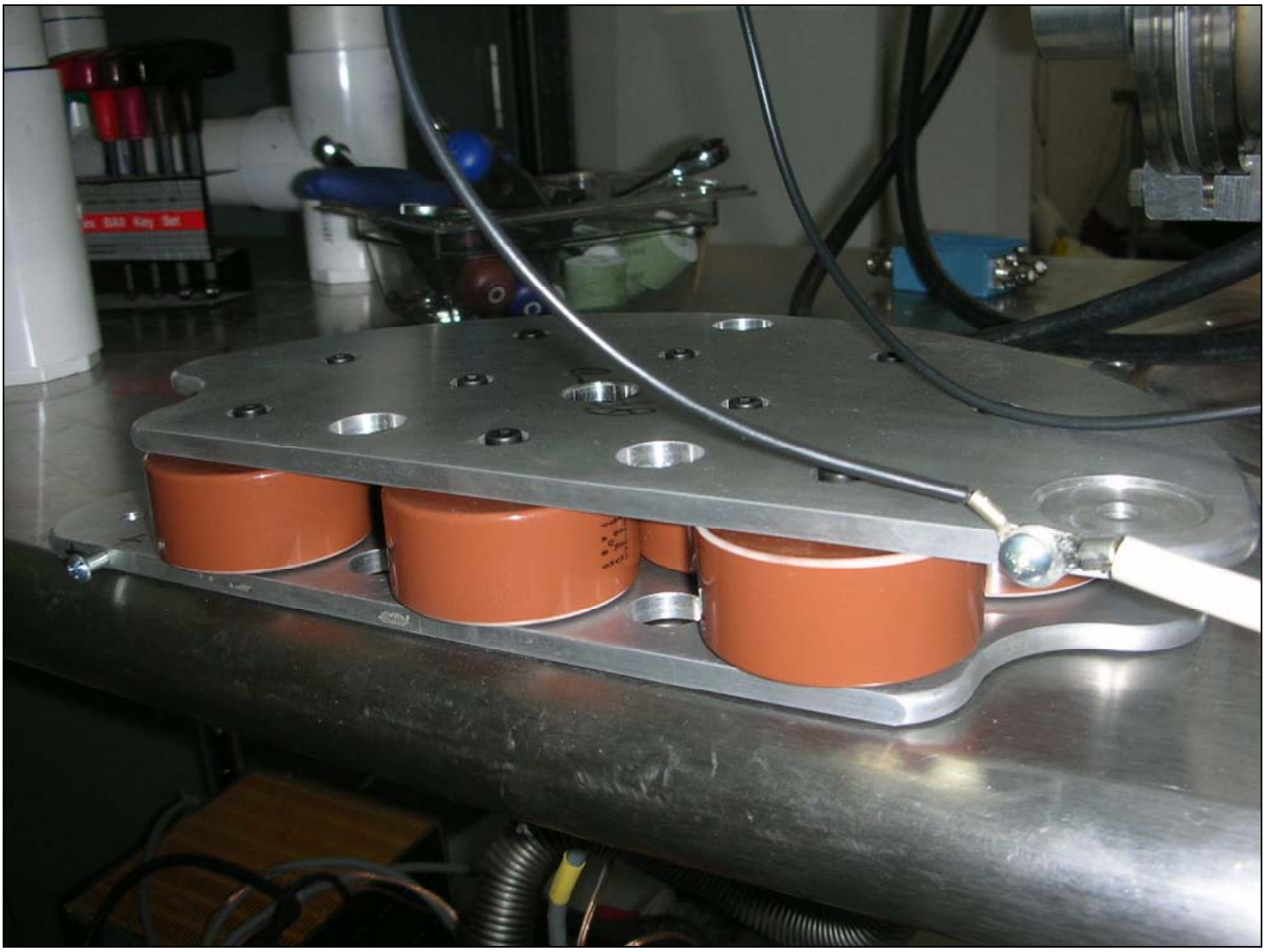

Figure 21 capacitor bank used to slow rise time

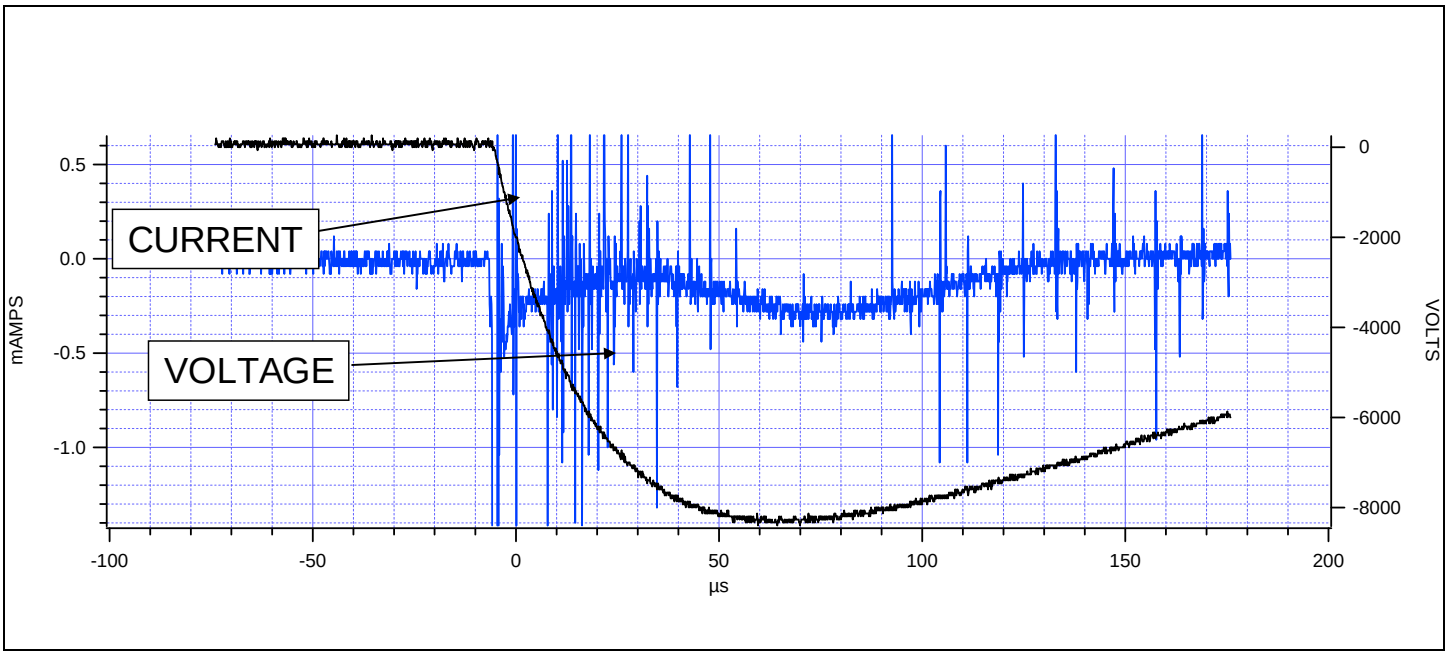

Figure 22 Typical slow rise time (40µS)

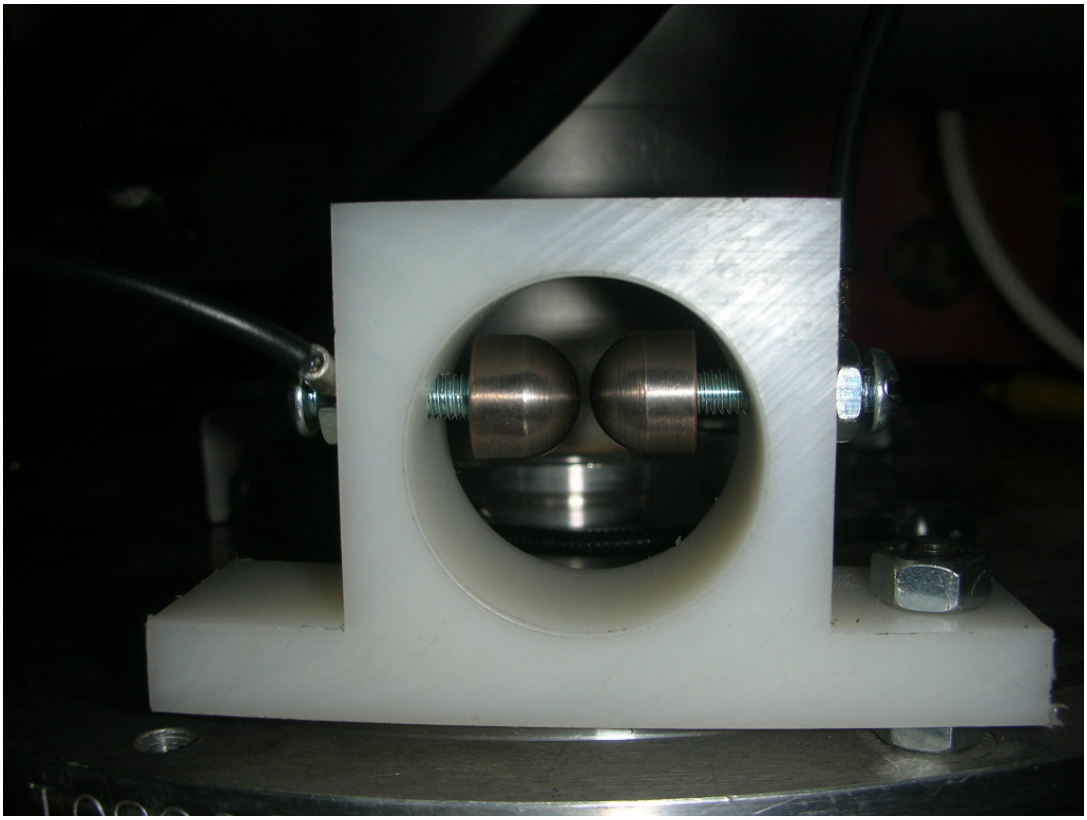

Figure 23 Laser triggered output switch to sharpen voltage pulse rise time

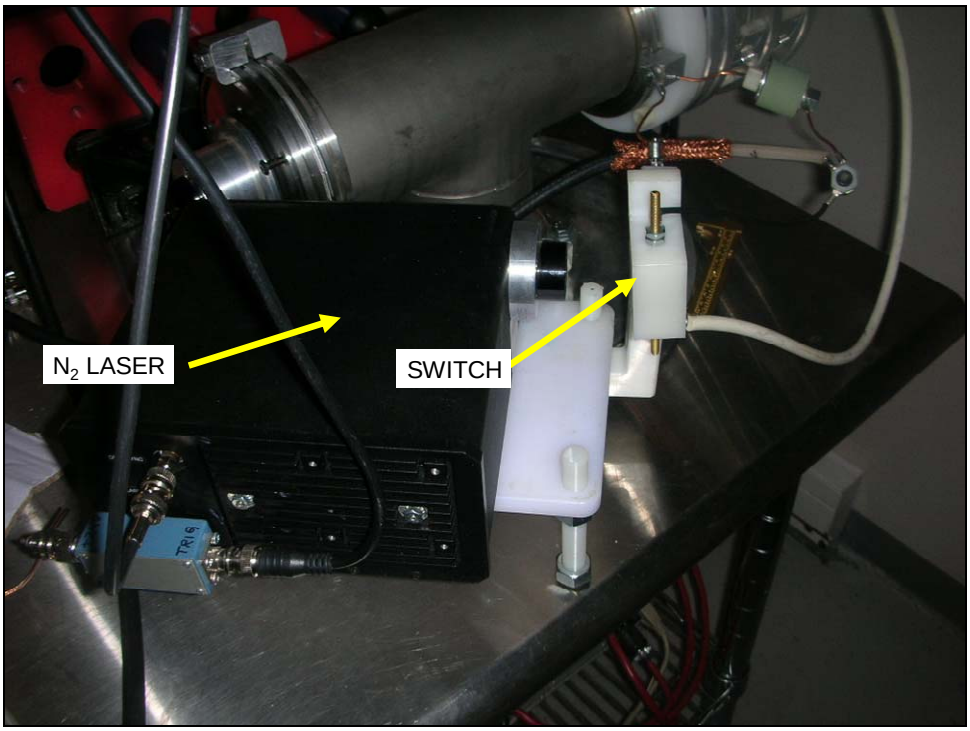

Figure 24 Laser trigger configuration showing laser, switch and load

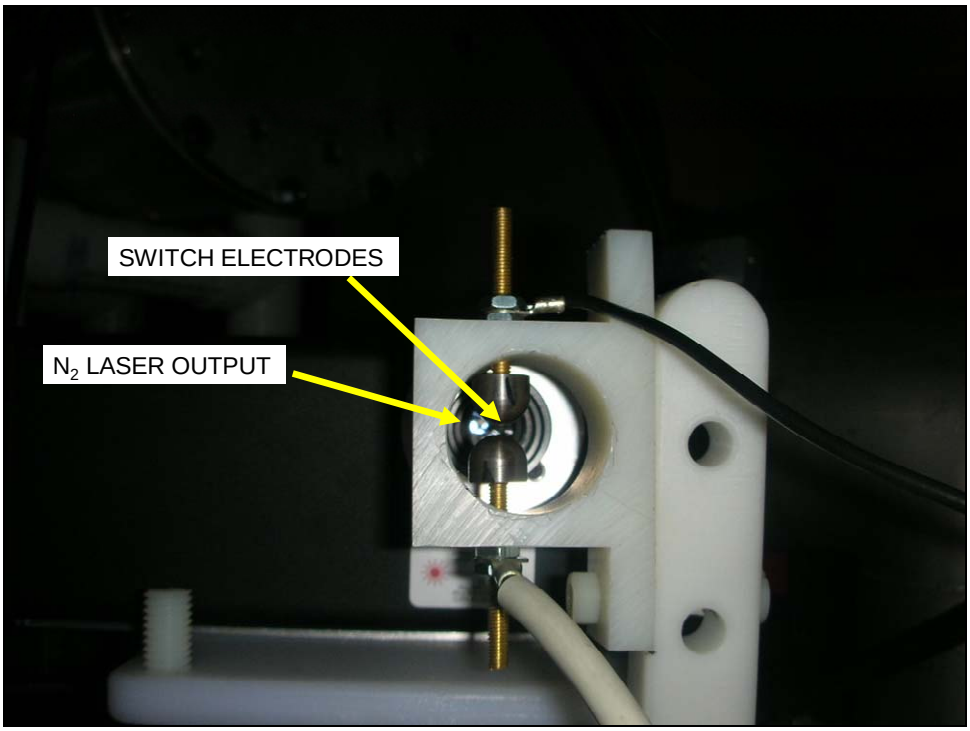

Figure 25 View of output switch illumination gap

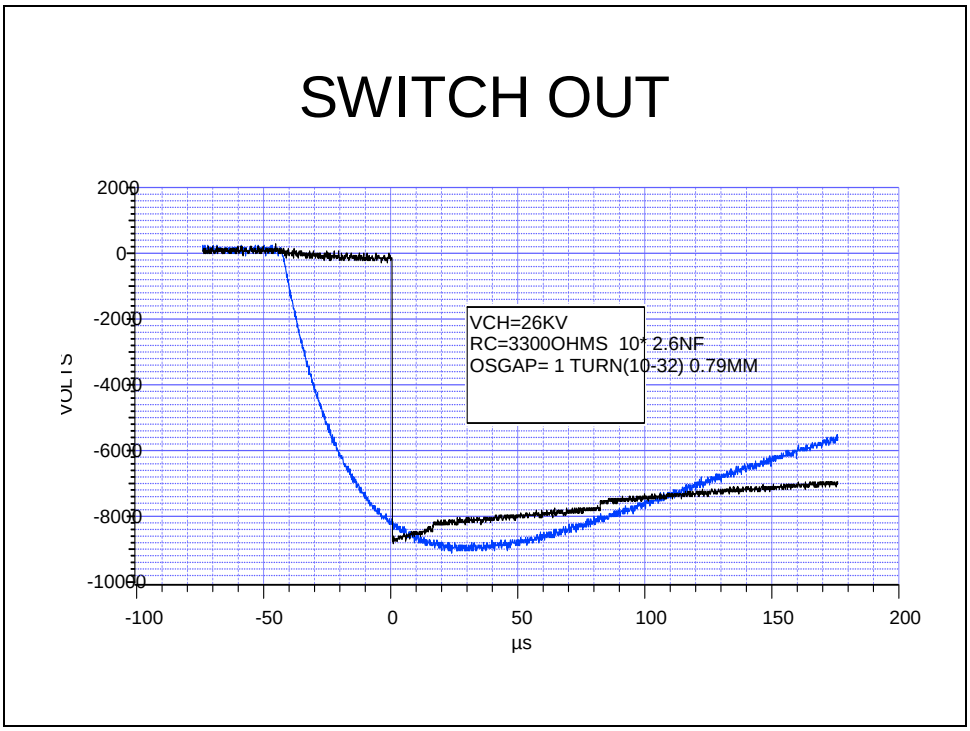

Figure 26 Output waveform showing very fast rise time (~15nS) into the load

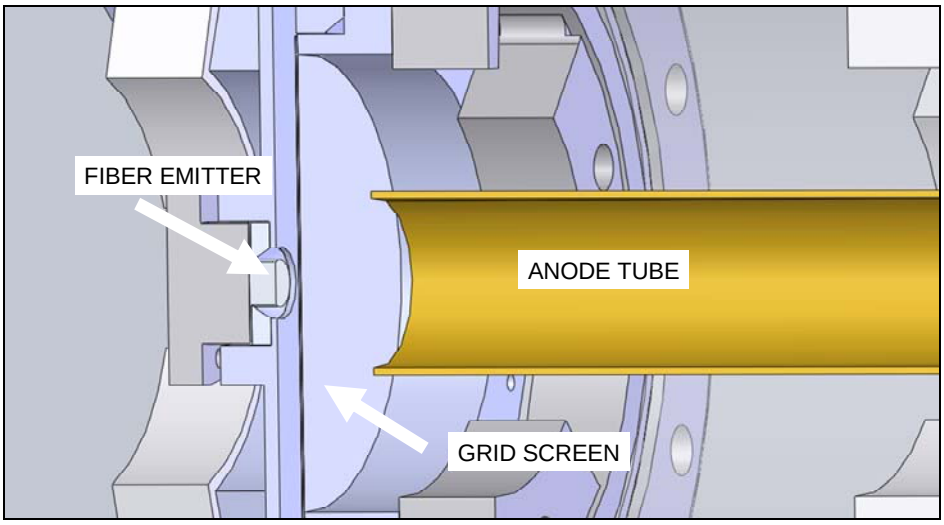

Figure 27. Cut-away view of extraction hardware

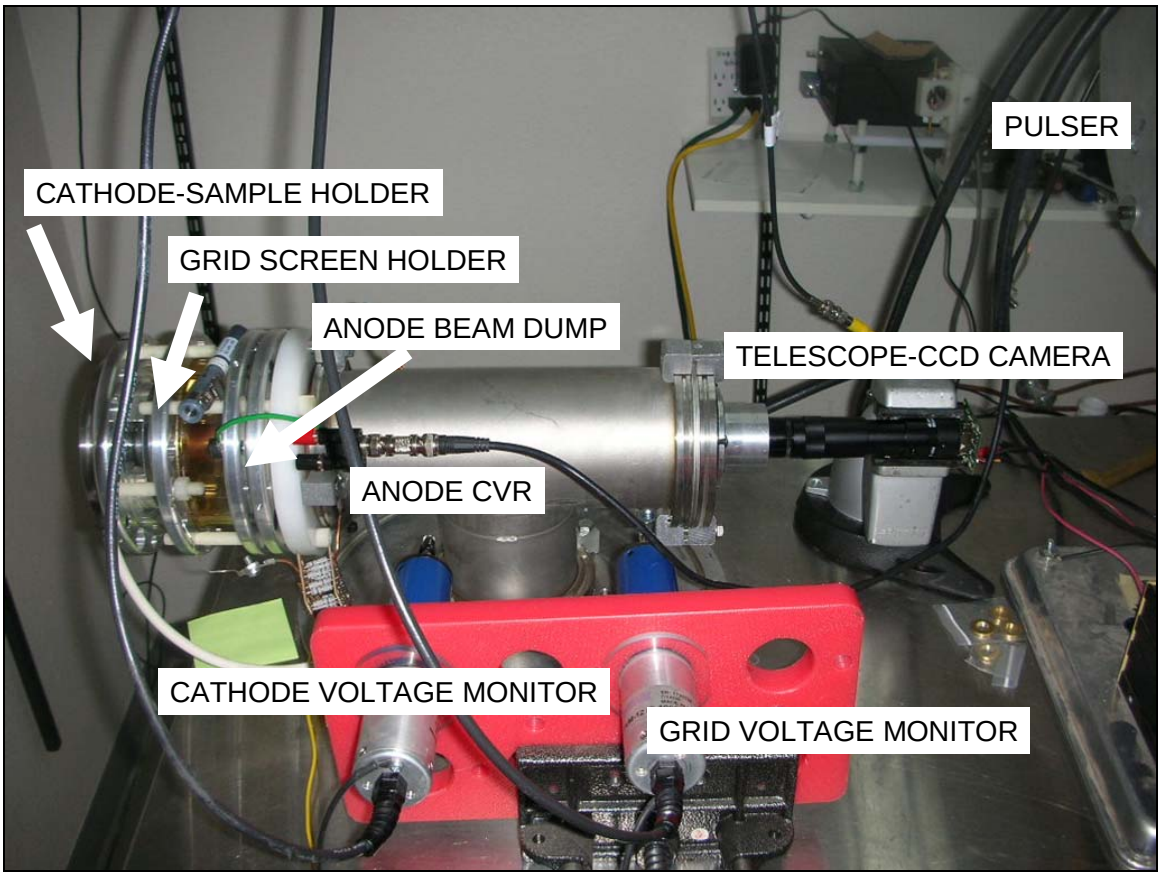

Figure 28 Experiment setup.

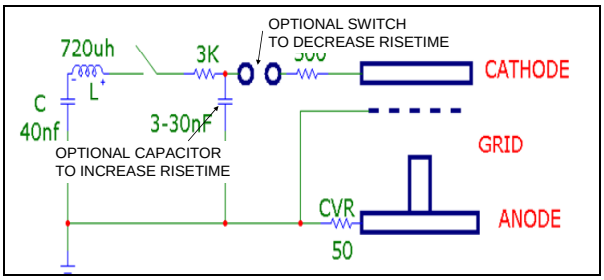

Figure 29. Experimental geometry

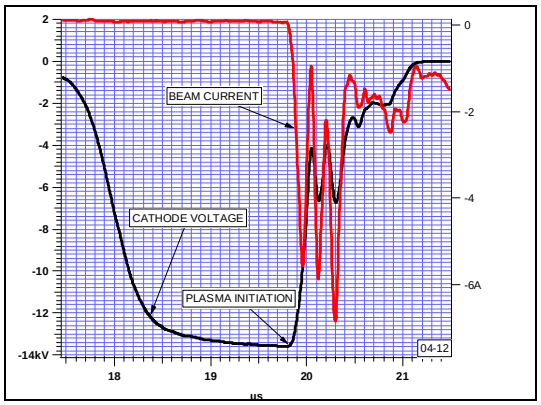

Figure 30. Electron emission: uncoated fibers, 4A, 500ns, 6mm/µS closure velocity

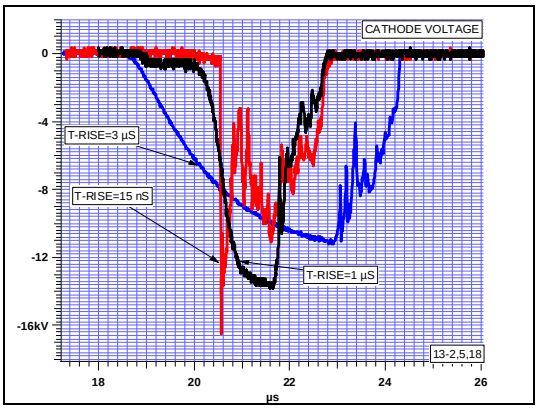

Figure 31. Rise time plasma threshold dependence in conditioned, un-coated fibers

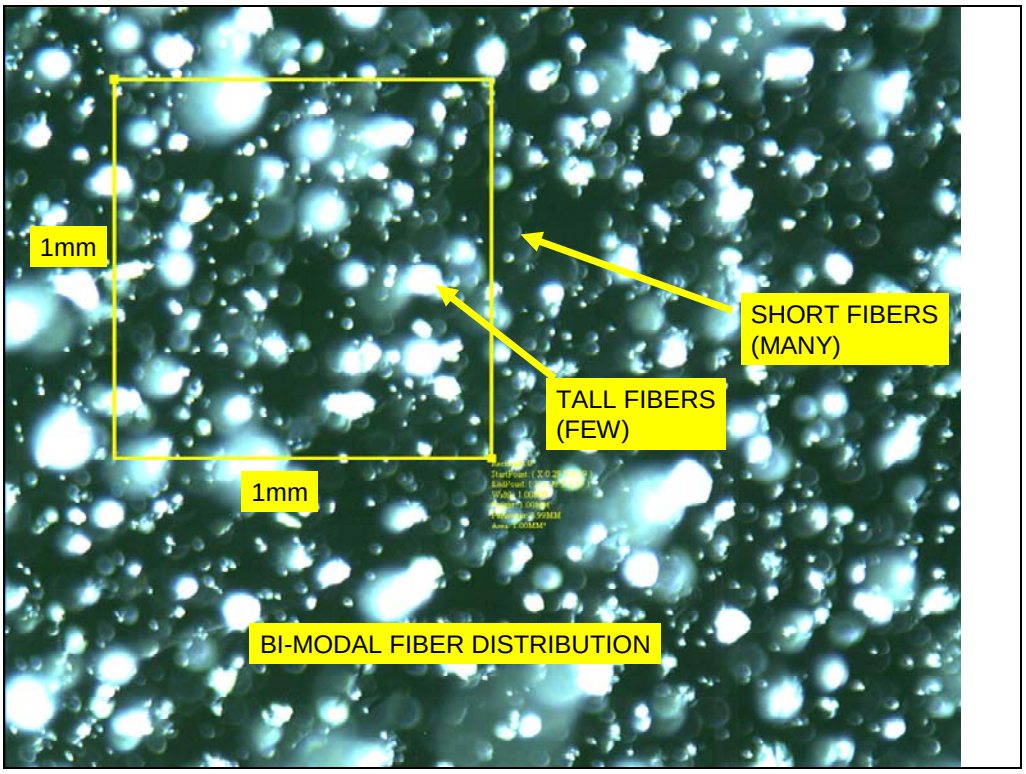

Figure 32. Micrograph: CSI coated emitter

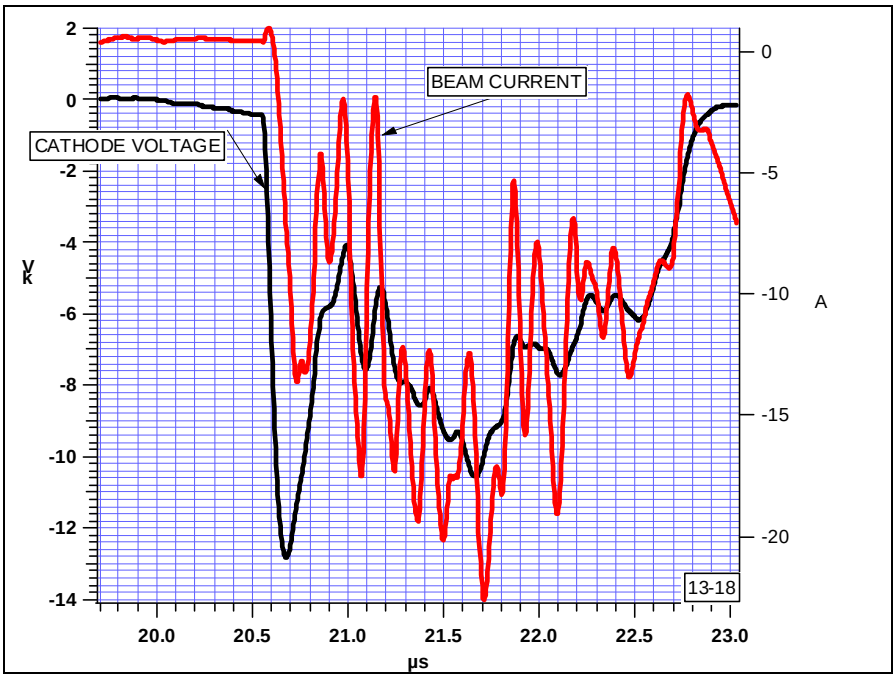

Figure 33. Electron emission: CSI coated fibers. 10A, 1.5μS, 2mm/μS closure velocity

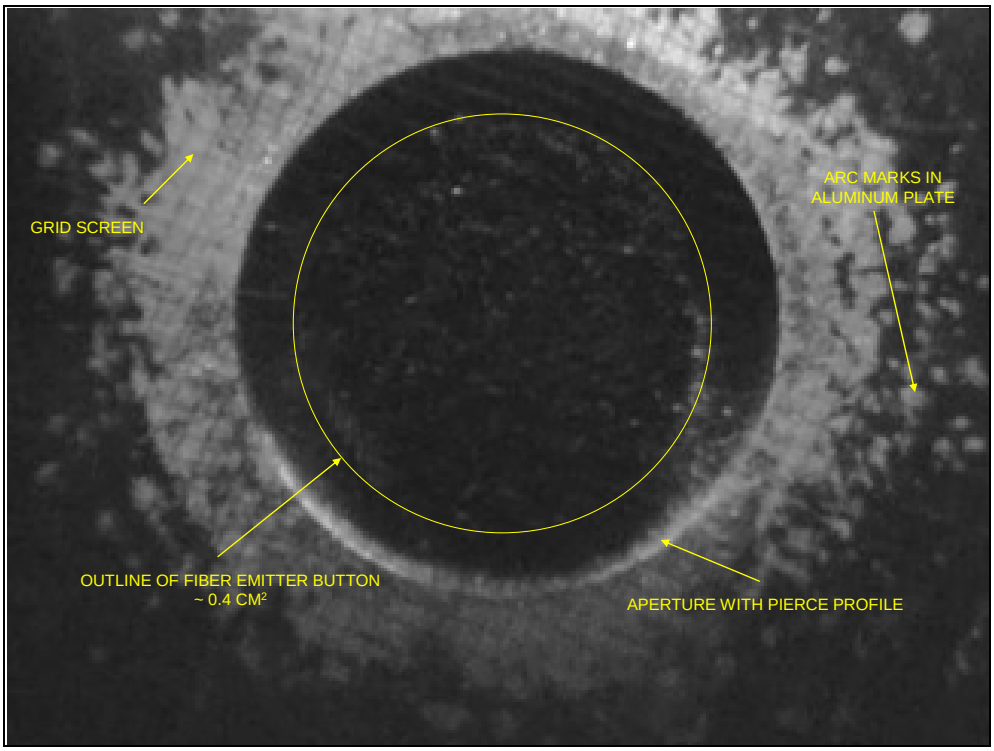

Figure 34. Telescope image: emitter through screen.

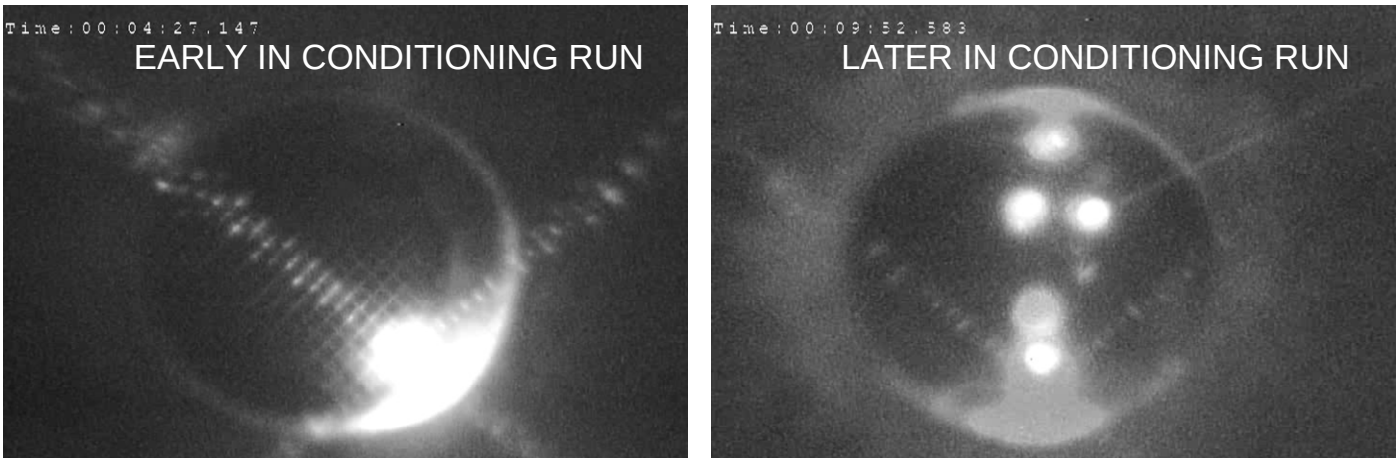

Figure 35 DC conditioning arcs.

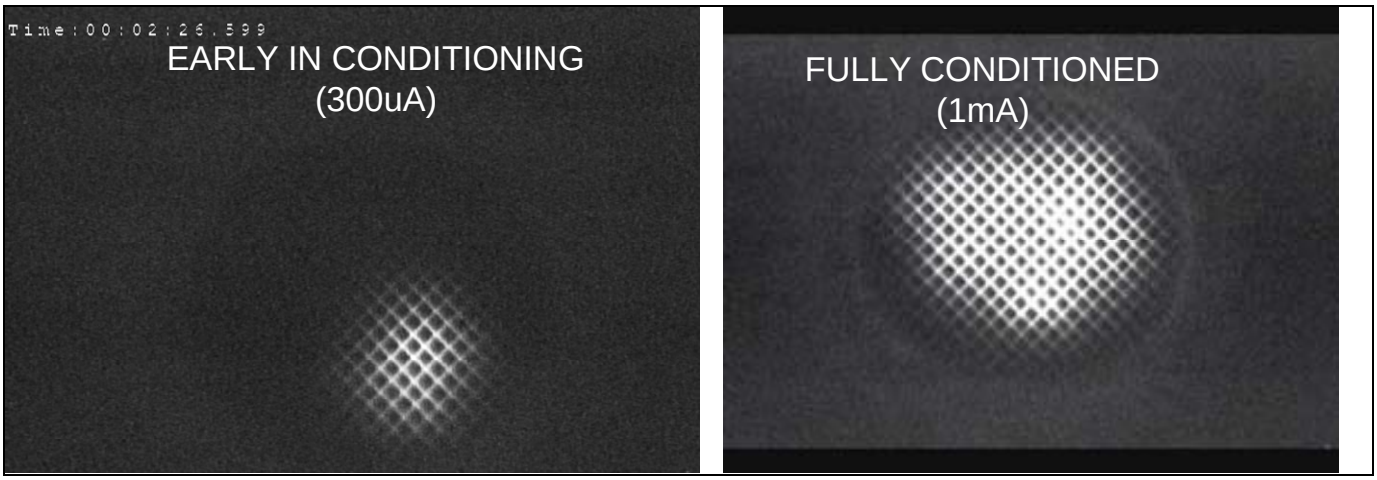

Figure 36. DC emission: grid glow from e-beam heating

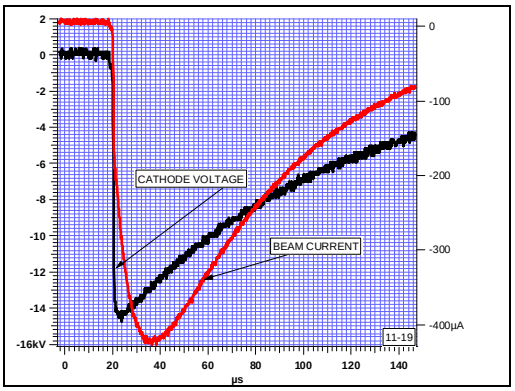

Figure 37. non-plasma, very long emission with conditioned, uncoated fibers.

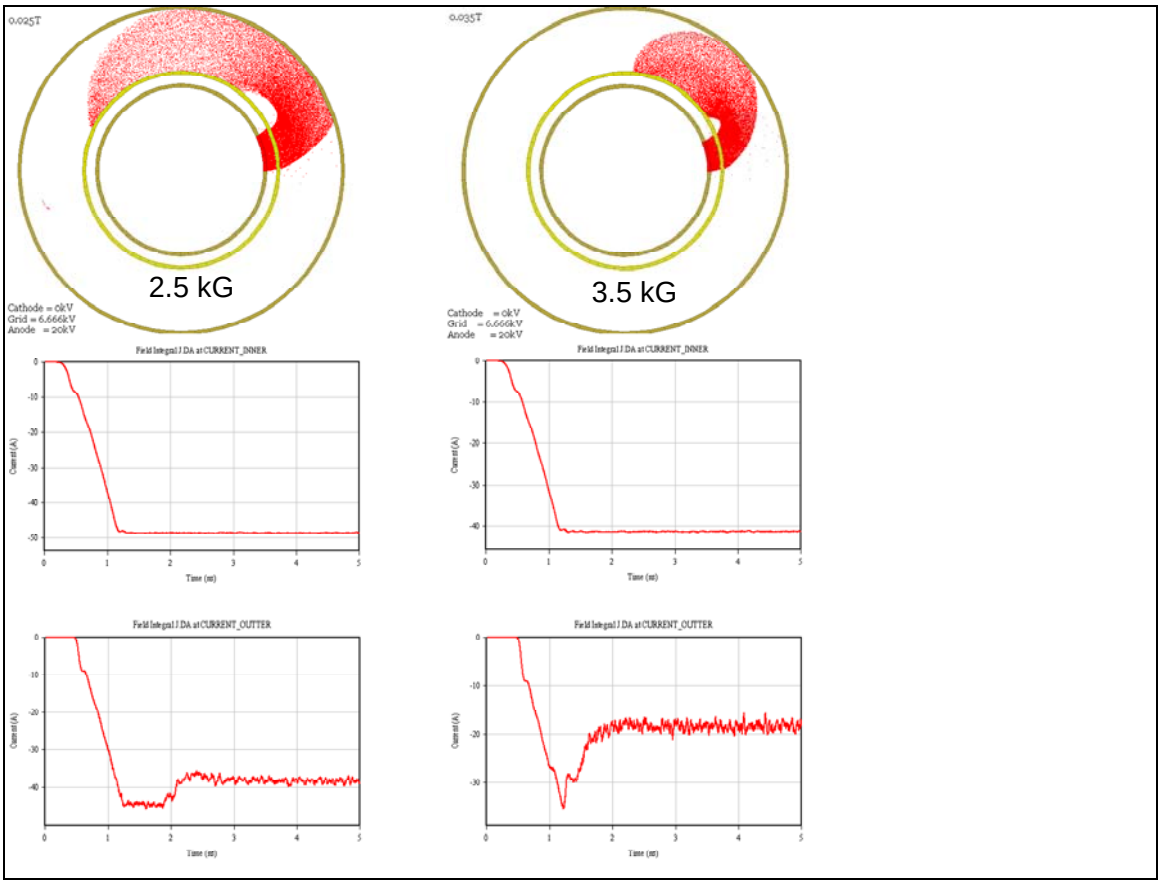

Figure 38. A6 simulation. Vk=0,Vg=7kv,Va=20kV.